The Astrophysical Journal, 841:69 (17pp), 2017 June 1 https://doi.org/10.3847/1538-4357/aa70a2

A New Approach to Convective Core Overshooting: Probabilistic Constraints from Color–Magnitude Diagrams of LMC Clusters

Philip Rosenfield[1,10], Léo Girardi[2], Benjamin F. Williams[3], L. Clifton Johnson[4], Andrew Dolphin[5], Alessandro Bressan[6], Daniel Weisz[7], Julianne J. Dalcanton[3], Morgan Fouesneau[8], and Jason Kalirai[9]
[1] Harvard-Smithsonian Center for Astrophysics, Cambridge, MA 02138, USA; philip.rosenfield@cfa.harvard.edu
[2] INAF Padova, Padova, Italy
[3] University of Washington, Seattle, WA 98105, USA
[4] University of California San Diego, San Diego, CA 92093, USA
[5] Raytheon Company, USA
[6] SISSA, Trieste, Italy
[7] University of California Berkeley, Berkeley, CA 94720, USA
[8] MPIA Heidelberg, Heidelberg, Germany
[9] Space Telescope Science Institute, Baltimore, MD 21218, USA
Received 2017 March 15; revised 2017 April 19; accepted 2017 April 30; published 2017 May 25

Abstract

We present a framework to simultaneously constrain the values and uncertainties of the strength of convective core overshooting, metallicity, extinction, distance, and age in stellar populations. We then apply the framework to archival *Hubble Space Telescope* observations of six stellar clusters in the Large Magellanic Cloud that have reported ages between ∼1–2.5 Gyr. Assuming a canonical value of the strength of core convective overshooting, we recover the well-known age–metallicity correlation, and additional correlations between metallicity and extinction and metallicity and distance. If we allow the strength of core overshooting to vary, we find that for intermediate-aged stellar clusters, the measured values of distance and extinction are negligibly effected by uncertainties of core overshooting strength. However, cluster age and metallicity may have disconcertingly large systematic shifts when Λ_c is allowed to vary by more than $\pm 0.05\ H_p$. Using the six stellar clusters, we combine their posterior distribution functions to obtain the most probable core overshooting value, $0.500^{+0.016}_{-0.134} H_p$, which is in line with canonical values.

Key words: Magellanic Clouds – stars: evolution – stars: interiors

Supporting material: figure sets

1. Introduction

Stellar evolution models are fundamental to nearly all studies in astrophysics. They play an important role in understanding the initial mass function (IMF) (e.g., Chabrier 2003), in determining line-of-sight extinction (e.g., Schlafly & Finkbeiner 2011), in measuring distances (e.g., via brightness of the tip of the red giant branch; e.g., Salaris & Cassisi 1997), in deriving supernovae rates and progenitor masses (e.g., Smartt 2015), and in measuring the cosmic star-formation history (e.g., Madau & Dickinson 2014). Unfortunately, some important aspects of stellar evolution remain poorly constrained and can impact the interpretation of galaxy observations (e.g., McQuinn et al. 2010; Melbourne et al. 2012). These aspects, such as mixing due to rotation or convection, are too complex to be derived from first principles and can only be constrained by observations.

The strongest observational constraints on stellar evolution models come from resolving individual stars in stellar clusters (e.g., Gallart et al. 2005). Star clusters are excellent stellar physics laboratories because individually, they fill a narrow parameter space in metallicity, abundance, and age, allowing the calibration of aspects of physical models. Within the Galaxy, stellar model constraints benefit from precise measurements of surface quantities and abundances of many member stars, and in some cases the possibility of independent measurement techniques from asteroseismology, and reliable parallaxes (e.g., Torres et al. 2010; Overbeek et al. 2017). However, there are not many nearby clusters that are both easily observable and young or intermediate-aged. Nearby Galactic clusters also tend to have near-Solar metallicities, and derived model constraints must then be extrapolated for use in stellar populations elsewhere. This limitation can be partially ameliorated by studying extragalactic star clusters. The Large and Small Magellanic Clouds (LMC, SMC) contain resolvable stellar clusters that are useful for accessing sub-Solar metallicities typical of nearby dwarf galaxies and galaxies in the distant universe. The MCs provide a rich sample of stellar clusters over a broad range in cluster mass and age. The MCs are also close enough to resolve stellar cluster members several magnitudes below the main-sequence turn off (MSTO), either using ground-based telescopes for more massive clusters or using the *Hubble Space Telescope* (*HST*) for clusters in the denser regions of the MCs.

To assess stellar models, researchers fit isochrones or synthetic stellar populations to their observations (e.g., Girardi et al. 2009; Milone et al. 2009; Goudfrooij et al. 2011). Unfortunately, uncertainties from both models and observations are not always accounted for, and seldom are degeneracies between sources of uncertainty modeled or discussed (with the strong exception of the robust Bayesian analyses led by von Hippel et al. 2006). Figure 1 shows a schematic of how theoretical and observational parameters can shift (1) the morphology of an isochrone on an optical color–magnitude diagram (CMD) and (2) the (number density of a) luminosity function of a single intermediate-aged (∼1.5 Gyr) stellar

[10] NSF Astronomy and Astrophysics Postdoctoral Fellow.

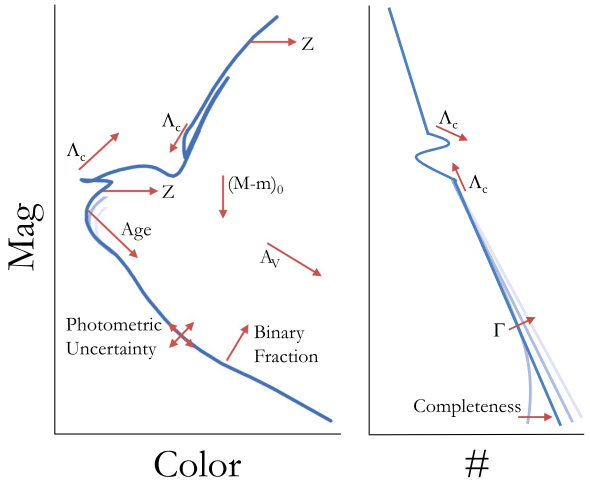

Figure 1. Schematic optical color–magnitude diagram (CMD; left) and luminosity function (right) showing how observational and theoretical uncertain parameters can change the morphology of an intermediate-age isochrone or synthetic stellar population drawn from isochrones and an IMF. Each arrow direction denotes approximate change with an increase in that parameter. An increase in photometric uncertainty and binary fraction will spread a star's location on the CMD, while the other shown parameters will shift the location of the isochrone. A probabilistic approach is needed to disentangle these effects.

population. Certain combinations of parameters, for example, distance modulus, μ_0, and extinction, A_V, could be construed as different age and metallicity, Z, of the cluster. One can choose other combinations of parameters in Figure 1 and create similar narratives, and each one would highlight the importance of simultaneously fitting all uncertain quantities to obtain stellar model constraints.

In this study, we focus on the strength of convective overshooting of the stellar core (Λ_c), i.e., the distance in pressure scale heights (H_p) a convective element may pass beyond the convective zone. Core convective overshooting is an important and uncertain process that effects the central H fusion lifetimes of stars $\sim$1.5–2.5$M_\odot$, a fundamental quantity in stellar evolution. Increasing the strength of core overshooting increases the main-sequence luminosity for a given stellar mass, hence partially mimicking the effect of a younger cluster age in models with weaker core overshooting.

This is the first in a series of papers from an *HST* archival program (AR-13901) to re-reduce and analyze $\sim$150 MC stellar clusters to obtain new constraints on stellar evolution models. Here we introduce a framework for using CMD fitting to find the most probable stellar evolution model by simultaneously fitting five observational and model parameters while taking into account observational uncertainties and completeness. As a first exploration, we apply our framework to six LMC clusters with MSTO stars that are expected to have convective cores, and therefore strong CMD signatures as a function of core overshooting strength. Our approach differs from typical isochrone fitting because we are able to use the posterior distribution functions (PDFs) to quantify the constraints on each parameter, as well as to see any correlations between parameters, whether they are observationally or theoretically uncertain.

In Section 1.1, we discuss theory and existing measurements of core convective overshooting in stars. In Section 2, we discuss cluster selection, followed by Section 3, where we briefly describe the data acquisition, reduction, photometry, and artificial star tests. In Section 4, we describe the stellar evolution model grid we built, the CMD fitting software MATCH, our prior distributions, and results from CMD fitting using the model grid and mock data. In Section 5, we discuss the derived cluster parameters when holding Λ_c at its canonical value and varying it. We conclude in Section 6. The data and software used to make Figure 3 and on are available for download at this URL: 10.5281/zenodo.570196. The software is maintained on github: https://github.com/philrosenfield/core_overshoot_clusters, and the full core overshooting model grid is available at this URL:10.5281/zenodo.570192. All magnitudes follow the VEGAMAG system.

1.1. Previous Observational Constraints on Core Overshooting Strength

The treatment of convection in the stellar interior affects the effective temperature, luminosity, and age of the MSTO in low-mass stars and the hot extension of the blue loop in intermediate-mass He-burning stars. Core overshooting affects different parts of a CMD differently, depending on the age of the stellar population. Constraining core overshooting is important in astrophysics beyond the goal of precision stellar evolution models because uncertainties in core overshooting strength can be of the order of 5% of the MS lifetime (τ_{MS}) for low-mass stars. At MC metallicities, 5% of an MS lifetime is a significant portion of subsequent evolutionary phases like the He-burning phase ($\sim$20% τ_{MS}) and thermally pulsating AGB phase (TP-AGB; $\lesssim$1% τ_{MS}). It is therefore a critical goal for those who study or use HB and TP-AGB models to push uncertainties in MS lifetimes smaller than the duration of the short-lived evolutionary phases after the MSTO.

Convection in stars is a complex, three-dimensional time dependent process, and while efforts are underway to apply 3D and 2D models of convection to 1D stellar models (e.g., Arnett et al. 2015), these techniques are still too computationally expensive to be applied across all stellar ages and masses needed to synthesize stellar populations. Instead, convective energy transport in 1D stellar models typically follows the mixing length formalism (MLT, Böhm-Vitense 1958), which defines the mixing length parameter α_{MLT}, as the mean distance a convective element travels before being reabsorbed into its surrounding medium. The Sun is the main target for calibrating α_{MLT} (e.g., Basu et al. 2009).

The formalism to describe convective overshooting differs between stellar modeling groups. The main two varieties continue the formalism of MLT and parameterize the strength of convective overshooting in units of pressure scale height (H_p). The PARSEC models (Bressan et al. 2012, 2013) define the parameter Λ_c across the Schwarzschild boundary (Bressan et al. 1981), while other groups adopt the parameter α_{ov} measured from above the Schwarzschild boundary. Whichever the preference, they can be compared following the relation, $\alpha_{ov} \sim \frac{\Lambda_c}{2} H_p$.

Observational constraints on core overshooting for masses $M \lesssim 3M_\odot$ historically come from by-eye fitting of isochrones to MSTO morphology of open clusters, after determining or adopting values for distance, reddening, and membership. The range of overshooting parameters fill in the range $0 \lesssim \Lambda_c \lesssim 0.5$, but are most commonly found to be 0.4 (e.g., Demarque et al. 1994; Kozhurina-Platais et al. 1997; Sarajedini et al. 1999; Woo & Demarque 2001). Bressan et al. (1993) suggested that Λ_c was not one value for all masses, and used $\Lambda_c = 0.25$ for

$1 - 1.5M_{\odot}$ and $\Lambda_c = 0.5$ for masses, $M \geqslant 1.5M_{\odot}$. A more gradual increase of the overshooting efficiency with mass was introduced by Demarque et al. (2004).

In the early 2000's, "by-eye" isochrone fitting was gradually supplemented with more robust analyses based on the comparison with synthetic CMDs and luminosity functions (e.g., Bertelli et al. 2003; Woo et al. 2003). This change in methods was enabled by the better photometric quality in the MCs with large telescopes and later with *HST*. These improvements were particularly important for studying MC clusters, which are generally more populated than their Galactic counterparts, and are often projected over sparely populated Galactic fields, hence reducing uncertainties related to low stellar counts and unknown membership probabilities.

Woo et al. (2003), using Yale isochrones (Yi et al. 2001), found the overshooting strength of $\Lambda_c \sim 0.4\ H_p$ to best-fit the CMDs of the intermediate-age LMC clusters NGC 2173, SL 556, and NGC 2155 (cluster ages ~1.5–3 Gyr; which would correspond to MSTO stars ~1.4–1.8 $M_{\odot}$ according to PARSEC models). Similar results were also obtained for NGC 2173 (Mucciarelli et al. 2007). Girardi et al. (2009) was able to simultaneously fit the dual red clump (RC) and MSTO in the center of the SMC cluster NGC 419 by adopting $\Lambda_c = 0.47^{+0.14}_{-0.04}$ and $\log\mathrm{Age} = 1.35^{+0.11}_{-0.04}$ Gyr (corresponding to an MSTO mass ~1.8 $M_{\odot}$) and assuming uncertainties dominated by random errors. At higher masses, the young LMC cluster NGC 1866 has produced independent evidence of moderate core overshooting (Barmina et al. 2002), though the findings have been challenged (see, e.g., Brocato et al. 2003).

Eclipsing binaries have also been used to measure core overshooting, through core overshooting's effect on stellar radius (e.g., Schroder et al. 1997; Ribas et al. 2000). The range in overshooting strength was found to be $0.48 \lesssim \Lambda_c \lesssim 0.64$ and increasing with increasing mass between 2.5 and 6.5 $M_{\odot}$. Claret & Torres (2016) found contradictory results from reanalyzing a well measured set of 33 double-lined eclipsing binaries in the Milky Way, LMC, and SMC. They found that Λ_c is independent of metallicity but depends on mass, such that Λ_c rises approximately linearly from 0 to 0.4 over the interval $1.2M_{\odot} \leqslant M \leqslant 2.0M_{\odot}$ and remains roughly constant for higher masses with a dispersion of ~0.06 (their sample reaches 4.4 $M_{\odot}$).

With the burst of asteroseismology observations, new avenues for observational constraints have found some of the most extreme non-zero values of core overshooting, (Deheuvels et al. 2010, $\Lambda_c = 0.34 \pm 0.06 H_p$ for a solar metallicity star with mass $M = 0.95M_{\odot}$) and the highest (Guenther et al. 2014, $\Lambda_c = 2$–2.5 for Procyon, $M \sim 1.5M_{\odot}$).

In summary, studies that are focused on individual stars are converging on convective core overshooting increasing with increasing mass at least up to masses of 6.5 $M_{\odot}$, while constraints from stellar populations find Λ_c values between 0.4 and 0.5 H_p. Reported uncertainties or dispersions of core overshooting strength are typically around the 15%–20% level or 0.06 H_p.

2. Cluster Selection

Clusters in our main program are described in detail in M. Fouesneau et al. (2017, in preparation). Briefly, we selected ~150 clusters by cross-matching MC cluster catalogs (Bica et al. 2008; Glatt et al. 2010; Baumgardt et al. 2013) with the *HST* photometric archive (i.e., observations taken with ACS, WFC3, and WFPC2 in at least two optical wide-band filters). From this sample, we selected six clusters (HODGE 2, NGC 1718, NGC 2208, NGC 2213, NGC 1644, and NGC 1795) with literature ages near 1.5 Gyr (Bica et al. 2008) that were distributed throughout the LMC (see Figure 2). Cluster ages were chosen to be near 1.5 Gyr because their MSTO stars will have convective cores, and therefore, the strength of core overshooting will most dramatically affect the CMD morphology of the MSTO and RC (discussed further in Section 4.1.2 below). In effect, clusters were re-reduced from two *HST* programs: GO-9891 (PI: Gilmore) and GO-12257 (PI: Girardi).

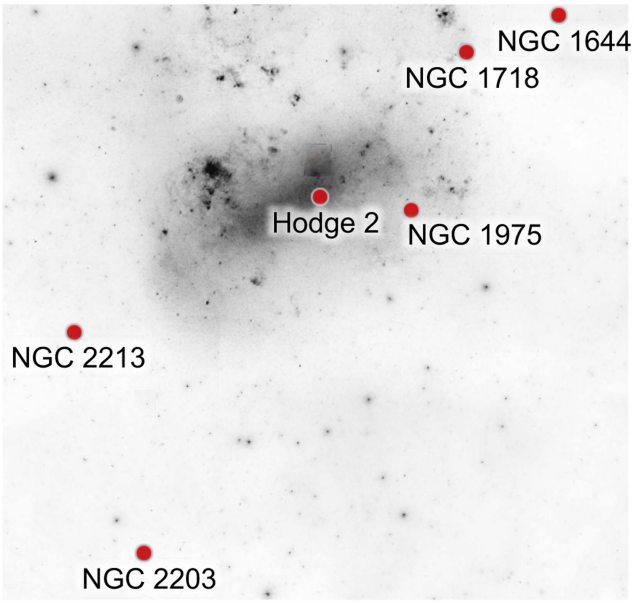

Figure 2. Sky distribution of stellar clusters.

The selected clusters have masses ranging from $\sim 2.3 \times 10^4 - 1.3 \times 10^5 M_{\odot}$ (Baumgardt et al. 2013) and varying morphologies of the MSTO. Several clusters in the MCs have been discovered to have MSTOs that are extend in color and luminosity (eMSTO; e.g., Milone et al. 2009) rather than MSTOs that show a narrow morphology that are typical in Galactic globular clusters (see Kalirai et al. 2012). Four of the six clusters in our sample have been identified as having eMSTOs, whose origins are actively being debated in the literature (e.g., Milone et al. 2009; Goudfrooij et al. 2011, 2014; Correnti et al. 2014; Bastian et al. 2016). For simplicity, we quote measured eMSTO widths as age spreads. Literature values of cluster properties are summarized in Table 1.

3. Archival Observations

3.1. Photometry and Reduction

ACS and WFC3 archival data were re-reduced using the University of Washington data reduction pipeline, which was developed to reduce large *HST* programs, e.g., ANGST and PHAT (Dalcanton et al. 2009, 2012). Its current capabilities are described in detail in Williams et al. (2014). Briefly, `flt` and `flc` images were downloaded from the Mikulski Archive for Space Telescopes (MAST; flt for WFC3/IR; flc for ACS and WFC3/UVIS), astrometrically aligned using the cross-camera alignment software developed for PHAT as part of *astrometry.net*,

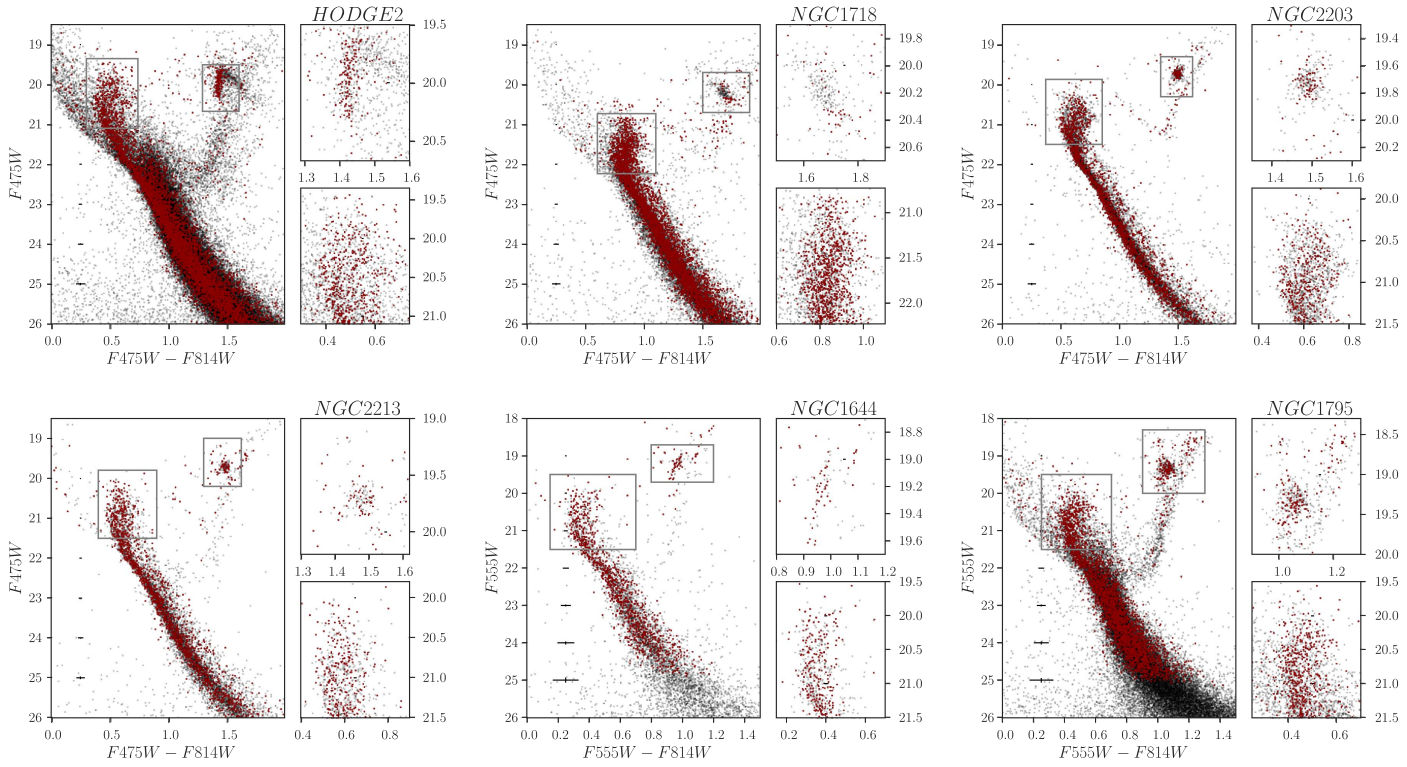

Figure 3. CMDs with insets MSTO (bottom) and HB (top) for each cluster. Black points are the full field `gst` catalog (Section 3) and red points are the stars with at least 70% cluster membership probability (Section 4.2.1). Mean photometric uncertainties are shown on the left side of each CMD.

Table 1
Cluster Parameters from Isochrone Fitting in the Literature

Name	log Mass ($M_\odot$)	Metallicity (Z)	μ_0	A_V	Age (Gyr)	eMSTO (Myr)	Reference	Stellar Model
(1)	(2)	(3)	(4)	(5)	(6)	(7)	(8)	(9)
Hodge 2	4.98	**0.008**	18.45	0.19	1.45		1	PARSEC
		0.008	18.40 ± 0.03	0.15 ± 0.02	1.30 ± 0.05	363	2	Padua08
NGC 1718	5.10	**0.008**	18.54	0.53	1.75		1	PARSEC
		0.008	18.42 ± 0.03	0.58 ± 0.03	1.80 ± 0.05	406	2	Padua08
		$0.008^{+0.002}_{-0.001}$	18.73 ± 0.07	0.31 ± 0.09[a]	2.04 ± 0.14		3	Padua02
NGC 2203	5.05	**0.008**	18.41	0.19	1.75		1	Padua08
		0.008	18.37 ± 0.03	0.16 ± 0.02	1.55 ± 0.05	475	2	PARSEC
		0.006	**18.49 ± 0.09**	0.34[a]	2.00 ± 1.1		4	PARSEC
NGC 2213	4.56	**0.008**	18.40	0.16	1.75		1	PARSEC
		0.008	18.36 ± 0.03	0.14 ± 0.02	1.70 ± 0.05	329	2	Padua08
		0.004 ± 0.001	18.56 ± 0.08	0.19 ± 0.09[a]	1.70 ± 0.14		3	Padua02
		0.006	**18.49 ± 0.09**	0.34[a]	1.78 ± 1.1		4	PARSEC
NGC 1644	4.32	0.008	18.48	0.03[a]	1.55	<50	5	BaSTI
NGC 1795	4.36	0.008	18.45	0.31[a]	1.3	<50	5	BaSTI

Notes. Reference for Column 2: Baumgardt et al. (2013). References and fitting notes for Columns 4–7: (1) Niederhofer et al. (2016)—μ_0 and A_V "by eye"; (2) Goudfrooij et al. (2014); (3) Kerber et al. (2007); (4) Piatti et al. (2014); (5) Milone et al. (2009)—"by hand." Stellar model references in Column 9: Padua08—Marigo et al. (2008); Padua02—Girardi et al. (2002); PARSEC—Bressan et al. (2012); BaSTI—An August 2008 version of Pietrinferni et al. (2004). Bold values denote fixed quantities during isochrone fitting. Uncertainties are included when available.
[a] $E(B-V)$ values were converted to A_V assuming $R_V = 3.1$.

and cleaned of cosmic rays using the *astrodrizzle* package (Gonzaga et al. 2012). We then used DOLPHOT (Dolphin 2000) for PSF photometry and created three photometric catalogs, `phot`, `st`, and `gst`, and we use the `gst` catalogs for our analysis. These catalogs provide three different levels of measurement quality. The `phot` catalogs are the closest to the full photometric output table from DOLPHOT. The `st` catalogs are culled from the `phot` catalogs and are limited to S/N $\geqslant 4$ and `sharpness`^{2} values in at least one filter to be below 0.2, 0.15 for ACS and UVIS respectively. The `gst` catalogs are a subset of the `st` catalogs that have `crowding` values below 1.3. CMDs of the `gst` catalogs are shown in black in Figure 3

Table 2
HST Archival Data

Target	Proposal ID	Instrument	Filter	Exposure Time (s)	Date
HODGE 2	12257	WFC3/UVIS	F814W	1430	2012 Jan 21
HODGE 2	12257	WFC3/UVIS	F475W	1440	2012 Jan 21
NGC 1718	12257	WFC3/UVIS	F814W	1430	2011 Dec 02
NGC 1718	12257	WFC3/UVIS	F475W	1440	2011 Dec 02
NGC 2203	12257	WFC3/UVIS	F814W	1980	2011 Oct 08
NGC 2203	12257	WFC3/UVIS	F475W	1520	2011 Oct 08
NGC 2213	12257	WFC3/UVIS	F814W	1430	2011 Nov 29
NGC 2213	12257	WFC3/UVIS	F475W	1440	2011 Nov 29
NGC 1644	9891	ACS/WFC	F555W	250	2003 Oct 07
NGC 1644	9891	ACS/WFC	F814W	170	2003 Oct 07
NGC 1795	9891	ACS/WFC	F555W	200	2003 Aug 09
NGC 1795	9891	ACS/WFC	F814W	300	2003 Aug 09

Note. Uniformly reduced archival observations retrieved from MAST.

Table 3
ASteCA-Derived Cluster Parameters

Cluster	α Center (J2000)	δ Center (J2000)	$r_{\rm cluster}$ (arcsec)	$\Delta_{\rm center}$[a] (arcsec)
HODGE 2	5 17 48.816 ± 0.048	−69 38 41.640 ± 0.720	33.84 ± 1.80	1.24
NGC 1718	4 52 25.704 ± 0.072	−67 03 05.040 ± 1.080	38.88 ± 2.52	4.06
NGC 2203	6 04 43.392 ± 0.072	−75 26 19.320 ± 1.080	42.12 ± 2.16	6.17
NGC 2213	6 10 42.240 ± 0.072	−71 31 45.840 ± 1.080	29.52 ± 2.16	2.13
NGC 1644	4 37 39.792 ± 0.096	−66 11 55.680 ± 1.440	26.28 ± 2.52	5.25
NGC 1795	4 59 47.280 ± 0.096	−69 48 03.960 ± 1.440	57.60 ± 2.88	6.58

Note.
[a] Separation between Bica et al. (2008) center coordinates and ASteCA-derived cluster center coordinates.

and the archival data are summarized in Table 2. Full details of our data reduction pipeline are postponed to our instrument paper (M. Fouesneau et al. 2017, in preparation).

3.2. Artificial Star Tests

In order to characterize the photometric errors and completeness of the *HST* data, we placed ∼100k artificial stars for each cluster. Artificial stars are distributed rather uniformly in CMD space covering the full magnitude and color range of the data, and weighted such that fainter mags have relatively larger numbers of tests. Artificial stars are distributed spatially according to a King profile, literature values for center and half-light radius, fixed concentration, covering a range in radius out to four half-light radii, and bounded by the ACS or UVIS field of view.

3.3. Cluster Parameters

We fed our gst catalogs into ASteCA (Perren et al. 2015), an automated stellar cluster analysis package, to estimate the cluster parameters and cluster membership. Table 3 lists the derived cluster centers, radii, and great circle distances between derived cluster centers and values from Bica et al. (2008).

Full details of the fitting algorithms are in the main ASteCA paper, in short, the cluster centers are determined by the maximum spatial density using a two-dimensional Gaussian kernel density estimator. The cluster radius is set to where the radial density profile becomes indistinguishable from the background stellar density. Contamination from non-cluster stars within the cluster radius are discussed in Section 4.2. Stars within the radius of the cluster and have at least 70% membership probability are used as input photometry and shown in red in Figure 3.

4. Methods

4.1. Stellar Evolution Models

The Padova–Trieste Stellar Evolution Code (PARSEC Bressan et al. 2012, 2013) is a major update to the Padua models (Girardi et al. 2000). PARSEC adopts the solar metallicity value of $Z_\odot = 0.01524$ and the scaled solar distribution of elements heavier than ^{4}He are taken from Grevesse & Sauval (1998) except for Li, C, N, O, P, S, K, Fe, Eu, Hf, Os, and Th, which are taken from Caffau et al. (2011) and references therein. The initial He abundance (Y_i) for each metallicity set is calculated based on the primordial He abundance, $Y_p = 0.2485$, (Komatsu et al. 2011) and the helium-to-metals enrichment ratio, $\Delta Y/\Delta Z = 1.78$, which was obtained in Bressan et al. (2012) using solar values. That is, $Y_i = Y_p + (\Delta Y/\Delta Z)\, Z_i$ (see Section 2 and Table 1 of Bressan et al. 2012).

PARSEC adopts an overshooting prescription that linearly increases in strength from no overshooting to the a maximum value ($\Lambda_{\rm max}$) between two mass steps (M_{O1}, M_{O2}). The Padua models (Girardi et al. 2000; Bertelli et al. 2008) set $\Lambda_{\rm max} = 0.5$, $M_{O1} = 1.0\ M_\odot$, and $M_{O2} = 1.5 M_\odot$ at all metallicities. In PARSEC V1.2S, $\Lambda_{\rm max}$ is the same; however, the mass steps are derived separately for each metallicity and helium content.

Table 4
PARSEC Convective Core Overshooting Model Grid

Parameter	Values
Mixture (Z_i, Y_i)	0.0005, 0.249
	0.0010, 0.250
	0.0020, 0.252
	0.0040, 0.256
	0.0060, 0.259
	0.0080, 0.263
	0.0100, 0.267
Λ_c (H_p)	0.3–0.6: $\Delta\Lambda_c = 0.1$
Mass ($M_\odot$)	$0.1 \leqslant M \leqslant 2.4$: $\Delta M \leqslant 0.05\ M_\odot$
	$2.6 \leqslant M \leqslant 6.4$: $\Delta M = 0.20\ M_\odot$
	$7.0 \leqslant M < 12.0$: $\Delta M = 1.0\ M_\odot$
	$12.0 < M \leqslant 20.0$: $\Delta M = 2.0\ M_\odot$

Note. We interpolated the overshooting grid to obtain $\Lambda_c = 0.45$ and 0.55 models and extended the grid to $\Lambda_c = 0.80$ for select clusters.

4.1.1. The PARSEC Core Overshooting Model Grid

We relax the PARSEC setting of $\Lambda_{\rm max} = 0.5$ and calculate a grid of 3,560 stellar evolution tracks using PARSEC V1.2S (updates from Chen et al. 2014; Tang et al. 2014) beginning at the pre-main sequence and ending at the termination of He-burning. Core overshooting in our model grid is not only calculated for hydrogen-burning (MS) cores, but helium-burning cores (HB or HeB) are also calculated with the labeled core overshooting strength. Table 4 lists the details of the stellar model grid.

4.1.2. The Effect of Core Overshooting

Increasing core overshooting strength allows more fresh nuclear material to fuse, making for a larger and hotter core that leads to a longer main sequence or HB lifetime and a brighter and cooler MSTO. We now describe how such a physical change in the interior of a star is expected to affect observations of a nearly single age stellar population. First, we illustrate how the core fusion lifetimes change, followed by the Hertzsprung–Russell diagram (HRD) and CMD appearance of sample stellar evolution tracks chosen at masses relevant to the ages of the sample clusters, and finally three simple synthetic stellar populations as snapshots of different epochs in star formation. As we will show, longer core fusing lifetimes translate to higher stellar densities on the CMD than otherwise expected. A brighter and cooler MSTO changes the expected position of a star on a CMD, leading to possible misidentification of a star's mass, age, or distance.

Figure 4 shows as a function of mass, the difference in core fusing lifetimes of core overshooting strength compared to the canonical PARSEC value ($\Lambda_c = 0.5\ H_p$). Solid and dashed lines mark the extrema of the stellar evolution model grid metallicities and are plotted for each calculated overshooting value (a similar comparison to other stellar modeling groups is discussed in the Appendix). The effect of core overshooting on MSTO age quickly increases from low masses to a peak, which is set by the linear ramp-up of core overshooting from the lowest masses in PARSEC. Soon after $\Lambda_{\rm max}$ is reached, the effect of the convective core on MSTO and He-burning age decreases, as expected, with increasing mass as core convection becomes less important. As an example, for a 1.5 $M_\odot$ star, an increase in core overshooting of $\Delta\Lambda_c = 0.1\ H_p$ leads to a

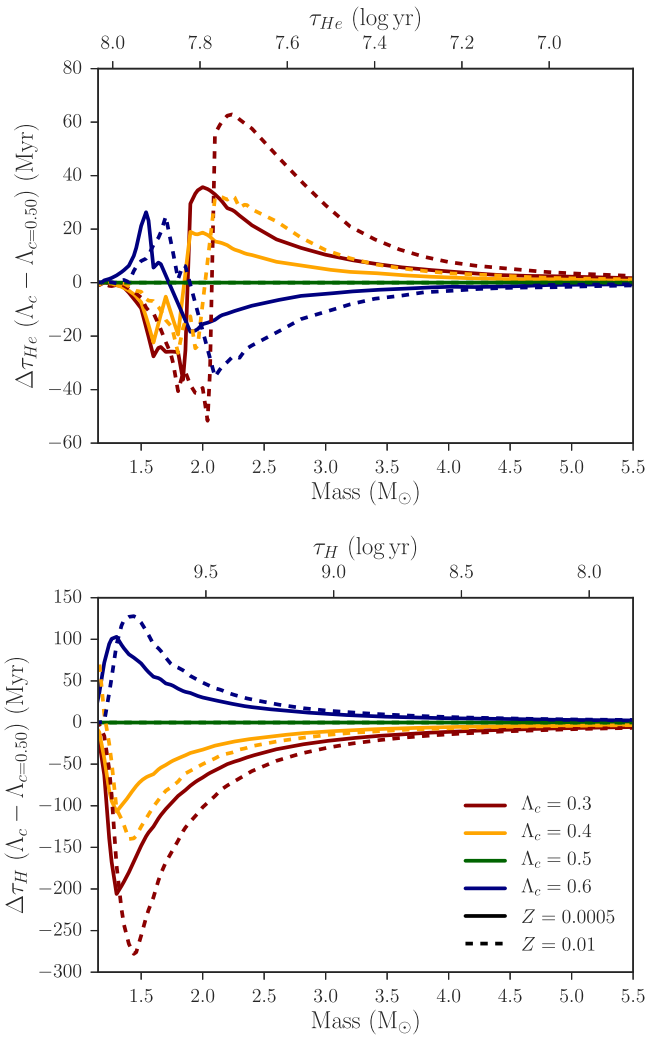

Figure 4. Increasing core overshooting increases helium burning (top) and main-sequence (bottom) lifetimes at masses around 1.5 $M_\odot$, when the convective core is largest. Shown are the differences, as a function of mass, in hydrogen-burning lifetime (i.e., MSTO age) and helium-burning lifetime of varying levels of core overshooting compared to the canonical PARSEC value of $\Lambda_c = 0.50\ H_p$. The solid and dashed lines denote the lowest and highest metallicities in the core overshooting model grid. Shown as a guide on the top axes of each panel are the H or He-burning lifetimes for $Z = 0.008$, $\Lambda_c = 0.50\ H_p$ models. Differences in MSTO lifetimes quickly increase until they peak at $\lambda_{\rm max}$, and increase once again for helium-burning stars that begin fusing helium in a non-degenerate state. A comparison to other stellar modeling groups is discussed in the Appendix.

∼100–150 Myr (∼5%) longer MS lifetime depending on metallicity. A ∼100–150 Myr increase in MS lifetime is a small effect for the MS; however, for a 1.5 $M_\odot$ star, it is longer than the entire core He-burning lifetime, and longer than the thermally pulsating AGB lifetime (e.g., Rosenfield et al. 2016).

Figure 5 shows an HRD (left panel) and a CMD (right panel) of evolutionary tracks from the core overshooting grid selected at initial masses of 1.5 $M_\odot$ and 2 $M_\odot$. The transformation from the HRD to magnitudes and colors are based on the tables of bolometric corrections from Girardi et al. (2008; revised for the latest ACS/WFC3 filter transmission curves) and rely on the ATLAS9 atmospheric models from Castelli & Kurucz (2004). The same transformations are also implemented in the `MATCH` routines (see Section 4).

The MSTO is shifted to brighter and to cooler effective temperatures with increasing core overshooting. However, the

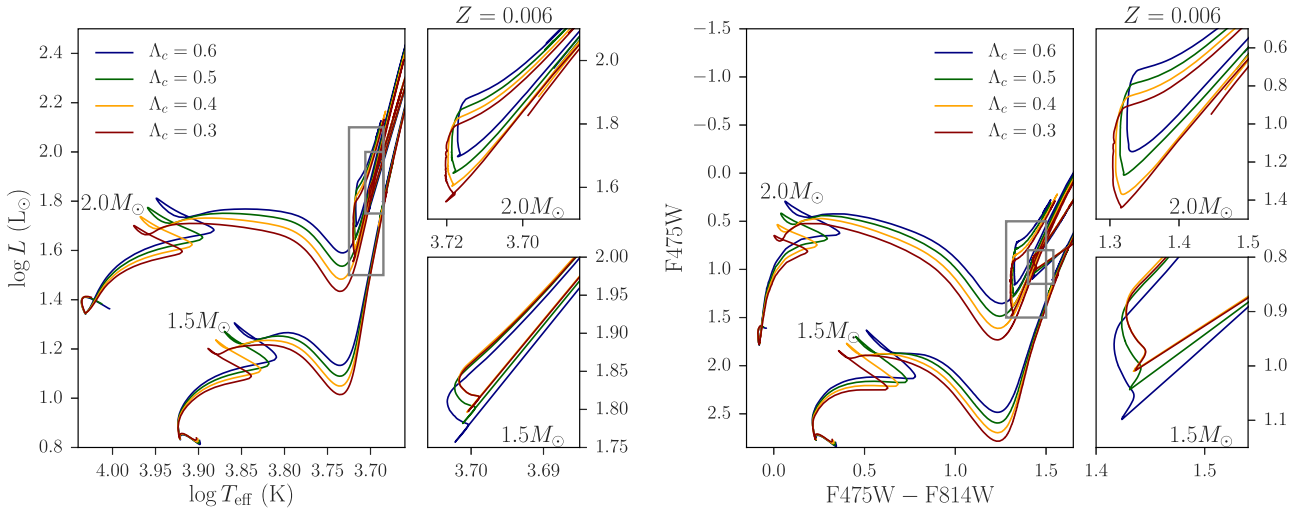

Figure 5. Left: Hertzsprung–Russell diagram (left) and CMD (right) showing model stellar evolutionary tracks at two masses with varying levels of core overshooting strength. Increasing core overshooting increases the luminosity and effective temperature of the MSTO to a lesser and lesser degree with increasing mass, changes the morphology of the SGB, and decreases the extent of the red clump. Insets: expanded views showing the helium-burning phases for each mass.

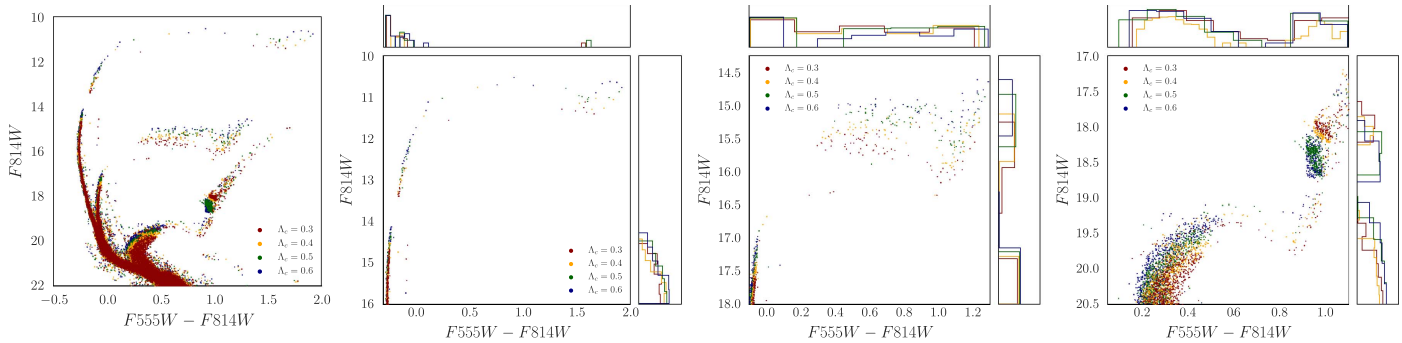

Figure 6. CMDs of synthetic stellar populations calculated at a distance of $\mu_0 = 18.5$, starting at three ages (14 Myr, 180 Myr, and 1.4 Gyr from left to right) and SF lasting 60 Myr, four values of core overshooting strength (red, yellow, green, purple for $\Lambda_c = 0.3$, 0.4, 0.5, and 0.6), and no binaries or extinction. Left-most panel is a combined summary of the right panels. Top and side axes of each of the three right panels show color and magnitude histograms. Each CMD shows increasing core overshooting strength, which increases the brightness of the MSTO. Other differences in morphology due to core overshooting differ with population age. In the center two panels, younger populations have fewer but brighter blue and red core He-burning stars (clumps of stars brighter than the MS and bluer or redder than F555W−F814W $\sim$ 0.75) with increasing overshooting. In the right panel, the morphology of both the MSTO and the RC differ with increasing overshooting strength as the MSTO and SGB are brighter while the RC is fainter and more populated.

amplitude of the brighter and cooler excursions decreases with increasing mass. There are also clear morphological differences around the MSTO, subgiant branch (SGB), and helium-burning phases. The extension between the minimum effective temperature on the MS and the MSTO increases with increasing core overshooting, the luminosity dip after the MSTO is more pronounced with increasing core overshooting, and the extent to hotter temperatures of the helium-burning tracks decreases with increasing core overshooting.

The age differences and the morphological changes in the stellar evolution tracks due to core overshooting strength culminate in the shape and number density of a stellar population on a CMD. Figure 6 shows synthetic stellar populations from models of each core overshooting strength produced using the `fake` routine in the `MATCH` package (see Section 4.2). The synthetic stellar populations are made of one burst of constant star formation lasting 60 Myr starting at 14 Myr (center left panel), 180 Myr (center right panel), and 1.4 Gyr (right panel), a constant initial metallicity of $Z = 0.006$ (corresponding to $[M/{\rm H}] = -0.40$ dex), a Salpeter (1955)

Table 5
Priors and the `calcsfh` Grid Search Space

Parameter	Range	Step Size
IMF (Γ)	1.35	(Salpeter 1955 fixed)
Binary fraction	0.30	(See Milone et al. 2009, 2016, fixed)
Distance (μ_0; mag)	18.3–18.7[a]	0.05
Extinction (A_V; mag)	0.0–0.5[a]	0.05
Age (Gyr)	1.0–2.5	0.06
Metallicity ([Fe/H]; dex)	−0.85 to 0.15	0.10
Core overshooting strength (Λ_c; H_p)	0.3–0.6[b]	0.1; 0.05 between $\Lambda_c = 0.4$–0.6
Color (mag)	$\sim$0.0–2.0 (varies by cluster)	0.05
Magnitude (mag)	$\sim$16–24 (varies by cluster)	0.10

Notes.
[a] NGC 1718 distance modulus prior was 18.5–18.9, and its extinction prior was 0.0–1 with the same listed step sizes.
[b] We extended the core overshooting grid to $\Lambda_c = 0.80$ for NGC 1718 and NGC 2203.

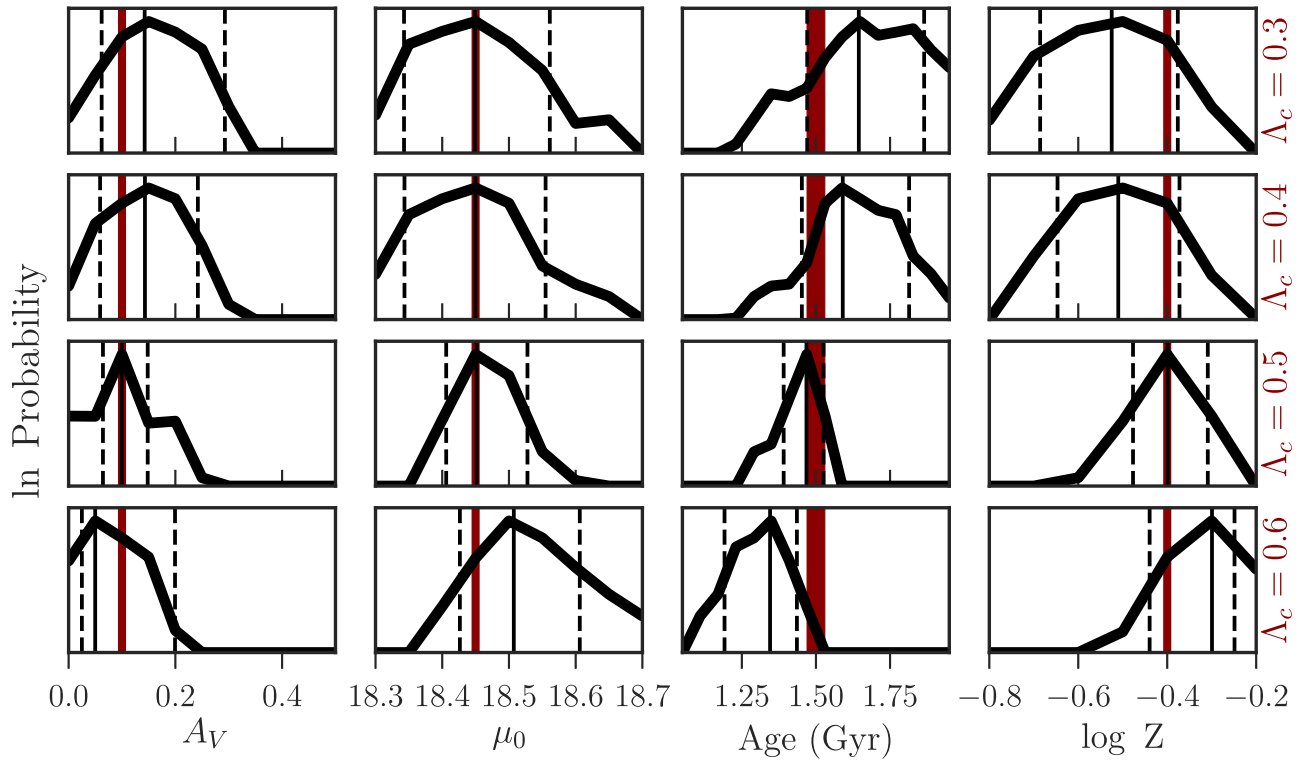

Figure 7. Marginalized PDFs of synthetic stellar populations derived with the canonical value of $\Lambda_c = 0.50$ H_p. The input stellar population parameters (truth) are shown in red, including the Λ_c value noted in the right-most panels. Dashed lines mark the 16th and 84th quartiles of the polynomial fit to the distribution and solid vertical black lines mark the maximum posterior probability. Incorrect assumptions on convective core overshooting strength will systematically offset derived cluster parameters. For a population with a mean age of 1.5 Gyr and SF lasting 60 Myr, uncertainties of the order of ± 0.05 H_p in Λ_c will introduce systematic offsets of $A_V \sim -0.04$ mag, $\mu_0 \sim +0.002$ mag, Age ~ -120 Myr, and log $Z \sim +0.01$ dex, with increasing Λ_c (see the text).

IMF, a distance $\mu_0 = 18.50$, typical photometric uncertainties, and neglecting binaries and extinction.

Figure 6 shows that observational signatures of core overshooting differ at different epochs of star formation. In the younger populations (center two panels) the core helium-burning stars show the most significant differences. Increasing overshooting strength decreases the extent of the blue loop, which manifests in the youngest CMD as brighter red and blue helium-burning stars (RHeB, BHeB; these stars have masses $>12M_\odot$ and $>3M_\odot$ in the center left and center right panels, respectively) with increasing overshooting. The numbers of RHeB and BHeB also decreases with increasing overshooting strength, which is more significant at the youngest aged population than the intermediate-aged population.

The oldest aged synthetic stellar population (right panel) exhibits different MSTO, SGB, and RC morphologies. Decreasing core overshooting strength increases the MSTO color, increases the number of SGB stars, lowers the total number of RC stars, and leads to a brighter, more compact RC.

4.2. CMD Fitting

CMDs are powerful tools for understanding the history of star formation in stellar populations. A CMD can be well approximated by a linear combination of bursts of star formation over cosmic time (Dolphin 2002). Exploiting the tenet, the `MATCH` software package (Dolphin 2016, and refs. therein), specifically, the `calcsfh` module was designed to derive the most likely SFH from a binned CMD (Hess diagram) of the photometry of a mixed-age stellar population.

To compare an observed Hess diagram to a model Hess diagram, `MATCH` first constructs the model Hess diagram given an input set of stellar models and user-specified prior on the IMF slope, binary fraction, metallicity, metallicity dispersion, and color and magnitude bin sizes. `calcsfh` will then iterate over distance, extinction, and epoch of SF burst, until either the most probable linear combination of ages is found (for mixed-age stellar populations), or until the likelihood is calculated for each epoch of SF (for near-single age stellar populations). We iterate calls to `calcsfh` to such that the single value priors become a distribution. We now describe how we set these prior distributions.

4.2.1. Prior Distributions

Table 5 lists our model priors and CMD fitting grid resolution. We chose our priors to be uninformative and flat distributions over a range set beyond derived literature values but limited for computational efficiency. We constrained values (IMF slope, binary fraction) that only effect the lower MS, where the photometric uncertainties are highest.

Binary Fraction—Observations of pre-MS stellar systems (e.g., Kroupa & Petr-Gotzens 2011), *N*-body simulations (e.g., Marks et al. 2011), and theoretical arguments (e.g., Goodwin & Kroupa 2005) suggest most stars are likely formed in binaries. The cluster radius, stellar type, cluster density, and age, among other factors contribute to the binary fraction. Sollima et al. (2007) found that the binary fraction varies from 0.1 to 0.5 for low-density Galactic globular clusters. Galactic field populations have measured binary fractions from ∼0.2 to 0.8 (e.g., Marks & Kroupa 2011, and references therein), with the

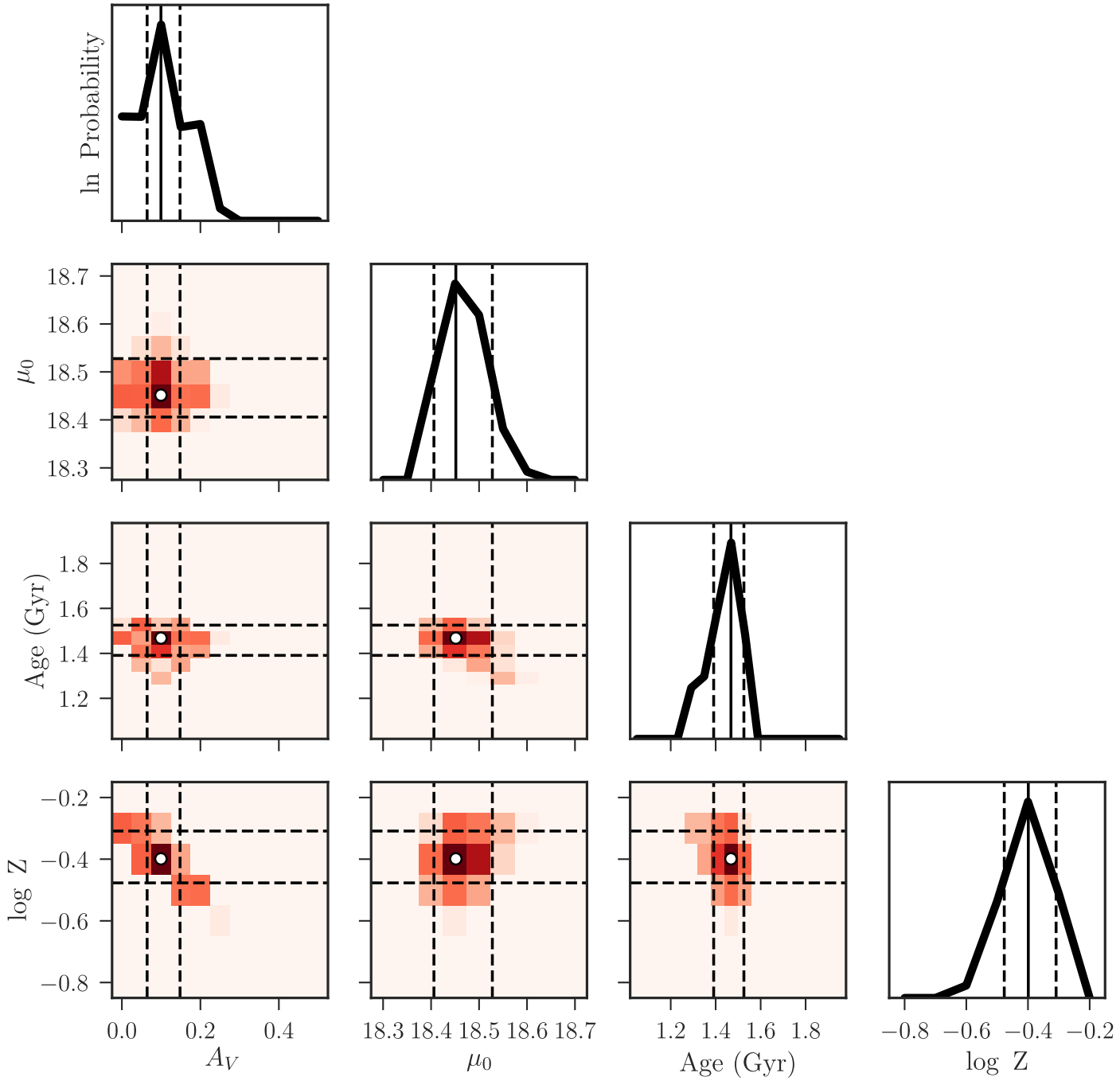

Figure 8. Joint-marginalized PDFs of a 1.5 Gyr ± 30 Myr stellar population calculated with $\Lambda_c = 0.5\ H_p$ and fit assuming $\Lambda_c = 0.5\ H_p$ (see third row of Figure 7). See Figure Set for PDFs with true Λ_c values mismatching the assumed value.

(The complete figure set (4 images) is available.)

fraction decreasing with decreasing stellar mass. In the MCs, Milone et al. (2009, 2016) determined the binary fraction ranges from ∼0.19 to 0.46 for several MC clusters. We set the binary fraction to the approximate median found in the Milone et al. (2009) papers, 0.3, with a uniform mass ratio distribution from 0.1 to 1.0$M_\odot$. We will explore variations of binary fractions in subsequent work that includes LMC and SMC clusters of differing age.

IMF Slope—We do not attempt to constrain the low-mass MS stars in this study, and adopt the Salpeter (1955) IMF slope of $\Gamma = 1.35$. The lowest mass stars to be included in our analysis have $M = 0.8\ M_\odot$.

Distance—We adopt a true distance modulus range of $\mu_0 = 18.30$–18.70 mag and step size 0.05 mag, which encompasses common literature values of $\mu_0 = 18.36$–18.54 mag with the exception of NGC 1718, which has a derived literature distance of 18.73 ± 0.07 (Kerber et al. 2007). Therefore, we extended the distance modulus range to 18.9 mag for NGC 1718 to ensure the best-fitting distance was not at the edge of the grid.

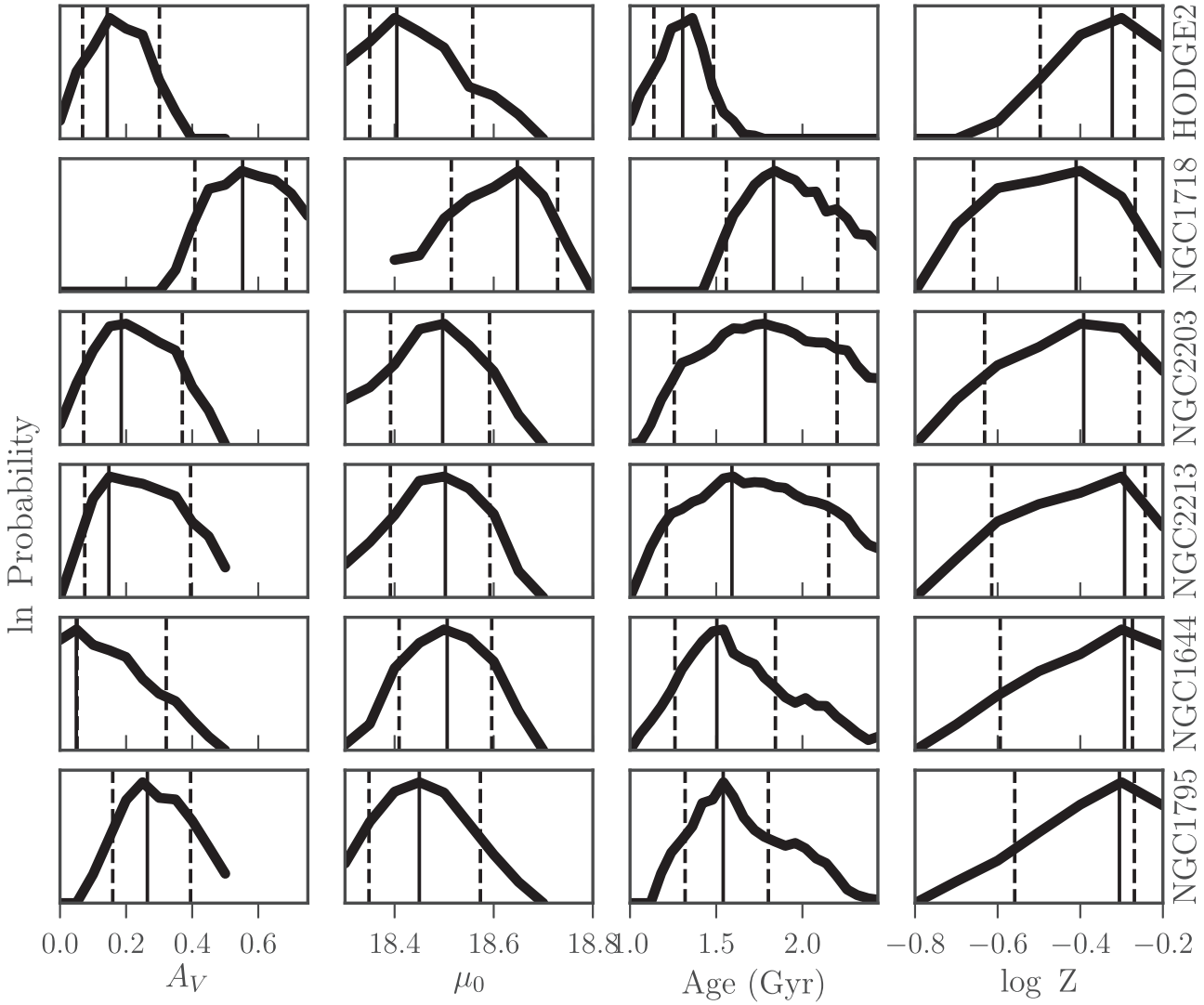

Figure 9. Marginalized PDFs derived with the canonical value of $\Lambda_c = 0.50$. Dashed lines mark the 16th and 84th quartiles of the polynomial fit to the distribution and solid vertical black lines mark the maximum posterior probability. Joint-marginalized PDFs are shown in Figure 10 and the figure set.

Extinction—Following the method to set our distance priors, values of A_V from the literature range from 0.03 to 0.58 mag. With A_V step size of 0.05 mag, we set our prior limits from 0 to 0.6 mag, again extending the grid edge for NGC 1718 to 1.0 mag.

Age—Clusters were selected because their literature ages were around 1.5 Gyr, we limited the age prior to 1.5 ± 0.75 Gyr for computational efficiency.

Metallicity—Most isochrone fitting of the clusters in our sample set the metallicity to either $Z = 0.008$ ([Fe/H] = −0.28 dex) or $Z = 0.006$ ([Fe/H] = −0.4 dex). We set our prior limits to $Z = 0.002$–0.01 ([Fe/H] = −0.85−0.15 dex) with a step size of 0.1 dex.

CMD Range and Binning—Using the simulated stellar populations described in Section 4.3, we ran `calcsfh` setting the color and magnitude bin sizes at all combinations of values 0.01, 0.05, 0.1, and 0.15 mag. We confirmed the heuristic tenet from Dolphin (2002): CMD bin sizes should be set smaller than the important observed CMD features, in our case, the MSTO and the HB. We adopt the color bin size of 0.05 mag and magnitude bin size of 0.10 mag.

Cluster Contamination—In the `ASteCA` package, the user may calculate the star-by-star probability of cluster membership by invoking a non-parametric Bayesian decontamination algorithm based on the method of Cabrera-Cano & Alfaro (1990), which was originally applied to open clusters. We limit the input photometry to stars within the cluster radius with at least 70% membership probability (shown in red in Figure 3).

Age and Metallicity Resolution—For stellar clusters, it is useful to measure the goodness of data-model fit of a simple stellar population (SSP) as a function of age. The minimum possible SSP age resolution in `MATCH` is set by an internal pre-compiled grid of partial CMDs, for our core overshooting grid this resolution is d[Fe/H] = 0.05 dex and dlog Age = 0.01 (log year). This high-resolution grid allows us to test SF in age bins $\gtrsim$20 Myr at ages of 1 Gyr (2%). However, we found there was no added improvement in the fitting between resolutions of 2% and 6%, so we adopted an SSP age resolution of 60 Myr because it provided an optimal balance between computational time and sensitivity to cluster age spreads.

4.3. Resolving Core-overshooting Strength in Synthetic Populations

We have seen that varying core overshooting strength propagates to CMD in ways that depend on age, which is the

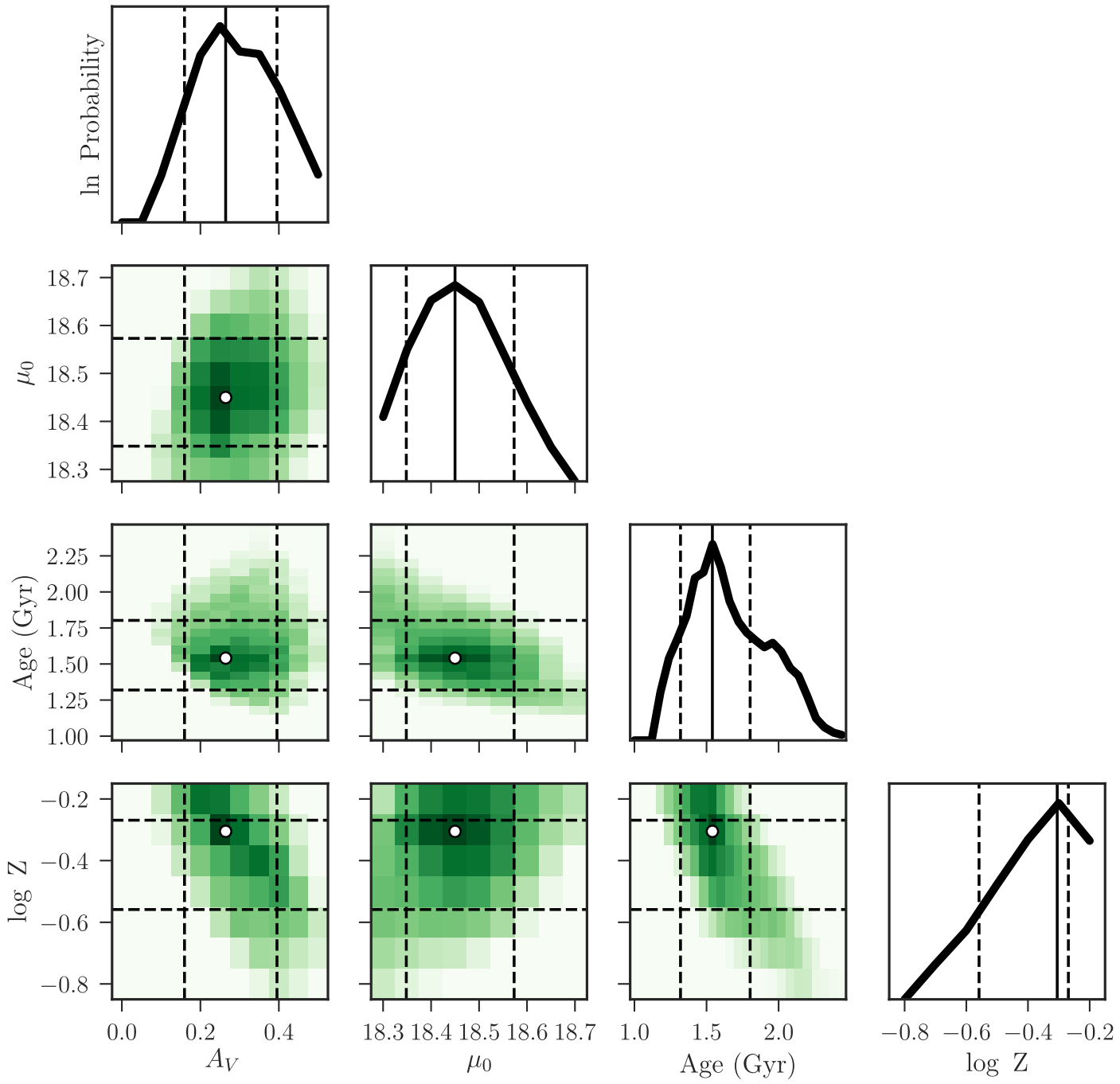

Figure 10. Joint-marginalized PDFs derived with the canonical value of $\Lambda_c = 0.50$ H_p for NGC 1795. Dashed lines mark the 16th and 84th quartiles of the polynomial fit to the distribution and solid vertical black lines on the diagonal panels mark the maximum posterior probability. The rest of the clusters are shown in the figure set.

(The complete figure set (5 images) is available.)

manifestation of the importance of convection in the stellar core (see Section 4.1.2). On an optical CMD, a stellar population that is brighter and cooler could mean that it is in fact closer and has less extinction than assumed. For example, it is tempting to point out that the F814W mag of the MSTO of the youngest synthetic population in Figure 6 shows ∼0.3 mag spread depending on the strength of core overshooting. These would correspond to bright stars with negligible photometric uncertainty. However, in these optical filter sets and at that population age, a large 0.3 spread in core overshooting strength at the MSTO is nearly indistinguishable from a ∼0.2 mag uncertainty in the distance modulus. This underscores the importance of using the entire CMD to test models of uncertain evolutionary phases. It also behooves us to test the sensitivity of CMD fitting and our core overshooting grid.

We ran the stellar population synthesis module `fake` within `MATCH` to simulate simple stellar populations. The `fake` module takes as input the same user-specified parameters as listed in Section 4.2, including artificial star tests to convolve with the model Hess diagrams and returns a synthetic CMD.

Table 6
Most Likely Cluster Parameters Given the PARSEC Model and Canonical Value of $\Lambda_c = 0.50\ H_p$

Cluster	A_V	μ_0	Age (Gyr)	Z
HODGE 2	$0.14^{+0.08}_{-0.16}$	$18.40^{+0.06}_{-0.15}$	$1.305^{+0.167}_{-0.179}$	$0.007^{+0.001}_{-0.002}$
NGC 1718	$0.55^{+0.15}_{-0.13}$	$18.65^{+0.13}_{-0.08}$	$1.833^{+0.274}_{-0.372}$	$0.006^{+0.002}_{-0.003}$
NGC 2203	$0.19^{+0.11}_{-0.19}$	$18.50^{+0.11}_{-0.10}$	$1.784^{+0.527}_{-0.417}$	$0.006^{+0.002}_{-0.003}$
NGC 2213	$0.15^{+0.07}_{-0.25}$	$18.50^{+0.11}_{-0.09}$	$1.591^{+0.381}_{-0.561}$	$0.008^{+0.001}_{-0.004}$
NGC 1644	$0.05^{+0.00}_{-0.27}$	$18.51^{+0.10}_{-0.09}$	$1.504^{+0.243}_{-0.340}$	$0.008^{+0.000}_{-0.004}$
NGC 1795	$0.26^{+0.10}_{-0.13}$	$18.45^{+0.10}_{-0.12}$	$1.541^{+0.221}_{-0.262}$	$0.008^{+0.001}_{-0.003}$

Note. Most likely cluster parameters listed are the maximum posterior probability, given our priors and assuming $\Lambda_c = 0.50$. Conservative uncertainties listed are the 16 and 84 percentiles of a polynomial fit to the posterior distributions (see Figures 9 and 10).

We ran `fake` to simulate a constant burst of SF at 1.5 Gyr $\pm$30 Myr, [Fe/H] $= -0.40$ dex, a metallicity dispersion of 0.10 dex, at each grid value of core overshooting strength, and convolved the CMD with a typical cluster artificial star test uncertainty profile.

Using the `MATCH fake` photometric catalogs as input to `calcsfh`, we derived the best-fitting CMD by searching over interstellar extinction, age, metallicity, and core overshooting strength (see Table 5). In all cases, that is, for each of the four mock data input catalogs, `calcsfh` clearly recovered the input parameters.

4.3.1. Likelihood

The best-fitting model is found by minimizing the Poisson-equivalent of χ^2 (see Dolphin 2002):

$$\chi^2_P = 2\sum m_i - n_i + n_i \ln\left(\frac{n_i}{m_i}\right), \quad (1)$$

where m_i is the number of model points and n_i is the number of data points in the Hess diagram bin i.

To visualize the likelihoods, we produce marginalized PDFs of each parameter, and joint-marginalized PDFs for each parameter pair. Joint-marginalized PDFs are comparable χ^2 maps for Gaussian distributions; in our case, they are χ^2_P maps.

The posterior distributions provide the full story of the uncertainties and correlations between parameters, given the PARSEC models and our priors. However, it is useful to note the most probable value and estimate the uncertainties for each fitted parameter. To do so, we report the "best fit" as the maximum posterior probability and take the 16th and 84th quartiles of a polynomial fit to posterior distribution as uncertainties. For a Gaussian distribution, these values would correspond to the mean and 1σ.

4.4. Systematic Uncertainties Due to Λ_c

To explore the effect of core overshooting strength on the derived cluster parameters, we marginalized the mock data results over the true value of Λ_c (i.e., Λ_c of the input synthetic stellar population) and the assumed value of Λ_c (i.e., Λ_c used to derive the cluster parameters).

Figure 7 shows the marginalized PDFs derived with an assumed value of $\Lambda_c = 0.50$ and all calculated true values. Red vertical lines show the (true) input values used to create the synthetic stellar populations, including the Λ_c values noted on the right vertical axes.

The systematic offsets introduced as a function of increasing true Λ_c follow from the discussion in Section 4.1.2 and Figures 4–6. For example, we have seen that increasing core overshooting strength increases core fusion lifetimes, therefore underestimating core overshooting strength will bias derived cluster ages older. This effect can be seen comparing the age panels in the top row and the third row of Figure 7 (the third row being where the assumed Λ_c matches the true Λ_c). We can further estimate the systematic offsets as a function of core overshooting strength expected for a population aged $\sim$1.5 Gyr. The median offsets of the maximum posterior probabilities are $A_V \sim -0.04$ mag, $\mu_0 \sim +0.002$ mag, Age ~ -120 Myr, and $\log Z \sim +0.1$ dex, when increasing Λ_c by $0.1H_p$. In other words, for intermediate-aged stellar clusters, distance, and extinction seem to be immune from uncertainties of core overshooting strength; however, age and metallicity may have disconcertingly large systematic offsets when Λ_c is uncertain by more than $\pm 0.05 H_p$.

Figure 8 shows the joint-marginalized PDFs when the assumed value matches the true value (the rest are in the figure set), and Figure 9 shows the marginalized PDFs. Effectively, this is a visualization of how well parameters can be recovered given a typical artificial star test uncertainty profile.

Using our core overshooting grid as the back-end stellar evolution models to `MATCH`, the `ASteCA`-derived cluster members as input photometry, and the artificial star tests to account for photometric uncertainty and completeness, we evaluate Equation (1) using `MATCH` or iterating calls to `MATCH` such that all combinations of parameters listed in Table 5 are searched.

5. Results and Discussion

5.1. Cluster Parameters with the Canonical PARSEC Model

Before exploring the effects of uncertain core overshooting strength, it is useful to understand the cluster parameter uncertainties and their correlations while assuming the canonical PARSEC value of $\Lambda_c = 0.50\ H_p$. In effect, this is a robust means to derive the cluster parameters if we were certain the most likely value of Λ_c was indeed $0.50\ H_p$.

Figure 10 shows the joint marginalized PDFs for each cluster assuming $\Lambda_c = 0.50\ H_p$ and the maximum posterior probabilities with the 16th and 84th quartiles of the distributions are listed in Table 6. The most likely parameters agree reasonably well with previous work (see Table 1) given the different stellar models, fixed parameters, and fitting methods. The best agreement between our derivation and that in the literature is Goudfrooij et al. (2014). Many of the derived values agree to within Goudfrooij et al. reported uncertainties and most derived values agree to within our more conservative $\sim 1\sigma$ constraints from the PDFs.

The main disagreements between Goudfrooij et al. (2014) and this work are in the fitting of NGC 1718, NGC 2203, and NGC 2213. Parameter differences for NGC 1718 and NGC 2203 are driven in part by the metallicity since Goudfrooij et al. select the best-fitting isochrone at either $Z = 0.008$ or $Z = 0.006$ and do not test intermediate values. For NGC 2213, the most likely metallicities agree, but we derive a distance of $\sim$0.7% farther (but closer to the mean LMC distance modulus of 18.49 ± 0.09 de Grijs et al. 2014)

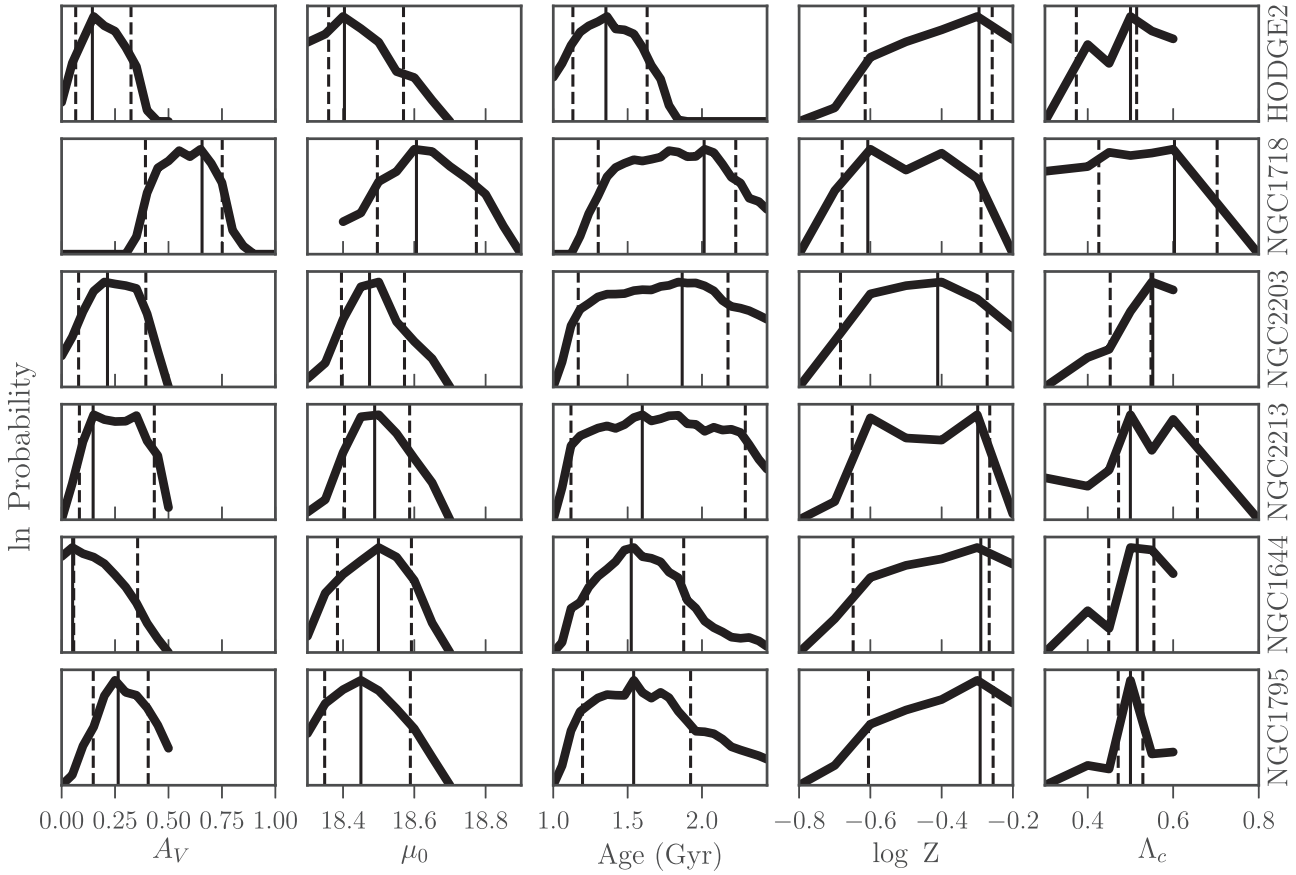

Figure 11. Marginalized PDFs on observational and physical parameters for each cluster. Dashed lines mark the 16th and 84th quartiles of the polynomial fit to the distribution and solid vertical black lines mark the maximum posterior probability. Joint-marginalized posteriors are shown in Figure 12 and the figure set.

and a most probable age of ∼100 Myr younger. We find the distance to NGC 1718 ∼1% farther than Goudfrooij et al. (2014) and ∼0.7% closer than Kerber et al. (2007), though beyond the mean LMC distance modulus.

Perhaps the most important aspect underlying the disagreements in cluster measurements are that these three clusters have eMSTOs. Determining the exact MSTO may be method dependent, especially for isochrone fitting. In other words, the nearly equal probable age over a span of ages evident in the PDFs make recovering the exact parameters difficult with the standard methods of isochrone fitting. The age-eMSTO connection reported in Goudfrooij et al. (2014) and others' work is recovered in the relatively extended widths of the marginalized age PDFs. Since the morphology of the MSTO is the clearest signal on a CMD of the underlying population age, a spread MSTO age would certainly manifest as a spread in color and magnitude around the MSTO. However, we refrain from commenting on the cause of the eMSTO until fully rotational models are included within this framework.

Regardless of the level of agreement between derived parameters, the joint marginalized PDFs (Figure 10 and Figure Set) reveal obvious correlations beyond the well-known age–metallicity relationship. Metallicity appears correlated with extinction, distance, and age for each cluster. At the very least, these findings should give hesitation to heavily weighting parameters reported from isochrone fitting methods that fix values before attempting to constrain other parameters.

5.2. Cluster Parameters Varying Λ_c

Relaxing the core overshooting strength prior has the effect of spreading all the PDFs, though no significant changes are seen in the maximum posterior probabilities (see Figure 11) with the exception of NGC 1718, which dropped 180 Myr in age and −0.2 dex in metallicity in order to land on its best-fit core overshooting value of $\Lambda_c = 0.6\ H_p$. The PDFs are also more complex compared to those in Figure 10. Core overshooting strength has a complex effect on CMDs, and some values of Λ_c seem to align well with different values of metallicity (e.g., NGC 2213). Asymmetric or lopsided PDFs are not signs of poor data quality or unreliable models, they are only signs that Gaussian and perhaps other functional approximations will likely inadequately describe the distribution.

The marginalized PDFs of convective core overshooting vary dramatically from cluster to cluster. For example, Figure 12 shows the joint marginalized PDFs for NGC 1795. There are clear peaks in each PDF denoting the maximum posterior probabilities, which are listed in Table 7. The general trends in correlations between parameters in the top four rows are very similar to in Figure 10 when Λ_c was fixed to the PARSEC canonical values. However, in the bottom row there are now correlations between Λ_c and other cluster parameters. The most apparent is the correlation between core overshooting and age. Next, there are slight correlations with Λ_c and distance and Λ_c and metallicity (the Λ_c-metallicity correlation is built into the PARSEC models). These correlations apparent in the

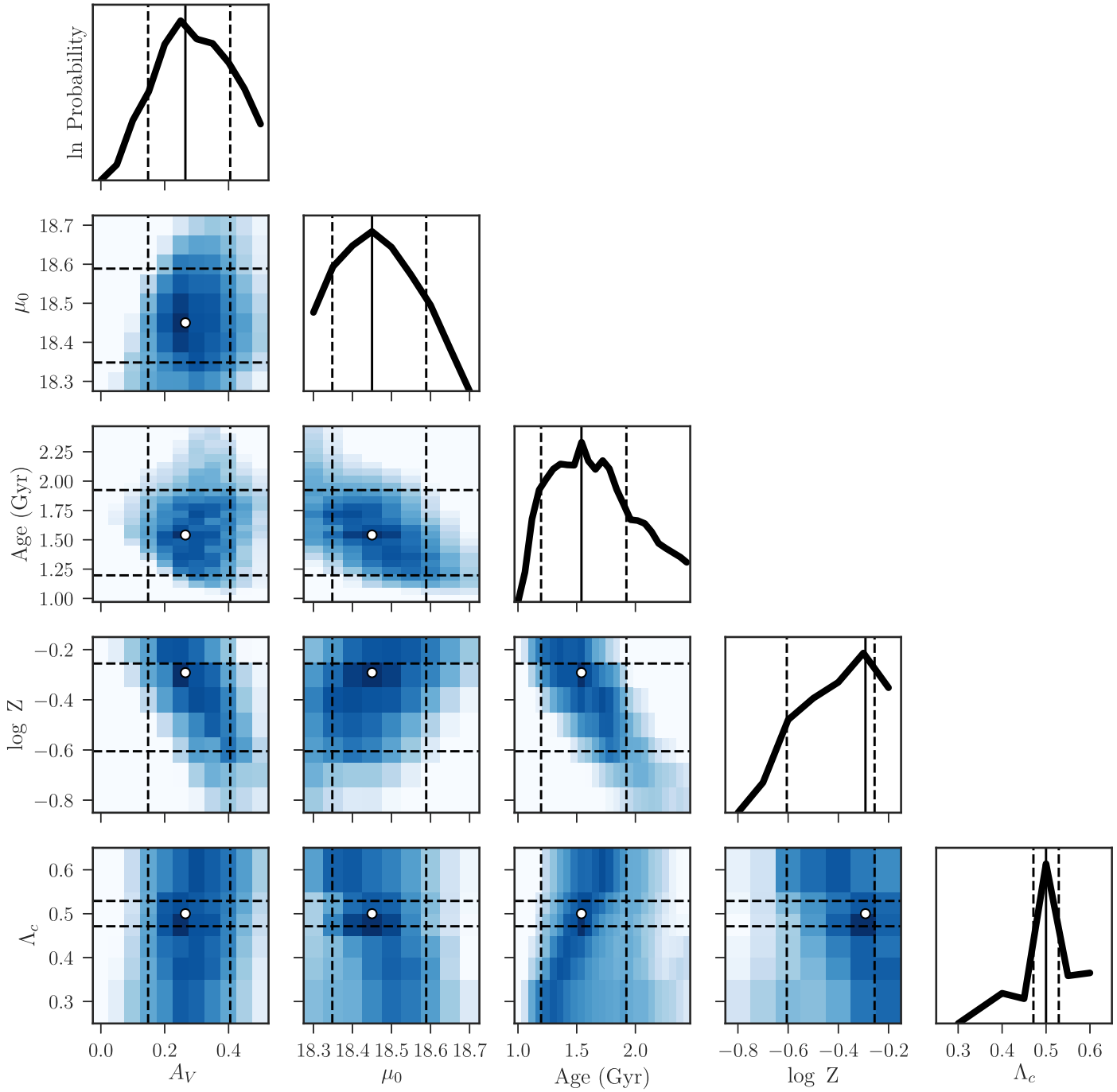

Figure 12. Joint-marginalized PDFs for NGC 1795. Dashed lines mark the 16th and 84th quartiles of the polynomial fit to the distribution and solid vertical black lines on the diagonal panels mark the maximum posterior probability. The diagonal panels for each cluster are the marginalized posteriors, shown together in Figure 11. The joint-marginalized PDFs for the remaining clusters are in the Figure Set.

(The complete figure set (5 images) is available.)

joint marginalized PDF of NGC 1795 are also seen in all other clusters (see the figure set).

One of many robust ways of discerning if the effect one measures is actually due to the parameter in question is by removing the parameter and re-running the analysis, and still understanding the results. By presenting our PDFs pedagogically, that is without varying core overshooting, and then by varying core overshooting, we have effectively done the necessary reliability test but in reverse. All the changes in the PDFs introduced by allowing core overshooting to vary are expected from the preceding discussion on the effects of core overshooting. For a couple clusters (e.g., NGC 2213), a higher value of overshooting with a lower value of metallicity fit nearly as well as the most probable values with canonical overshooting.

As discussed in Section 1.1, the emerging trend in recent studies focused on individual (or binary) stars is toward core overshooting strength increasing with increasing stellar mass (or age). It is interesting in this context that we find a strong correlation between age and Λ_c in exactly the same direction

Table 7
Most Likely Cluster Parameters Given the PARSEC Model

Cluster	A_V	μ_0	Age (Gyr)	Z	Λ_c
HODGE 2	$0.14^{+0.18}_{-0.08}$	$18.40^{+0.17}_{-0.04}$	$1.354^{+0.277}_{-0.222}$	$0.008^{+0.001}_{-0.004}$	$0.500^{+0.014}_{-0.127}$
NGC 1718	$0.66^{+0.09}_{-0.27}$	$18.61^{+0.17}_{-0.11}$	$2.015^{+0.213}_{-0.712}$	$0.004^{+0.004}_{-0.001}$	$0.603^{+0.100}_{-0.177}$
NGC 2203	$0.22^{+0.18}_{-0.14}$	$18.47^{+0.10}_{-0.07}$	$1.867^{+0.308}_{-0.699}$	$0.006^{+0.002}_{-0.003}$	$0.552^{+0.004}_{-0.100}$
NGC 2213	$0.15^{+0.29}_{-0.06}$	$18.49^{+0.10}_{-0.08}$	$1.599^{+0.693}_{-0.480}$	$0.008^{+0.001}_{-0.004}$	$0.500^{+0.157}_{-0.028}$
NGC 1644	$0.05^{+0.30}_{-0.01}$	$18.50^{+0.09}_{-0.11}$	$1.524^{+0.353}_{-0.294}$	$0.008^{+0.000}_{-0.004}$	$0.516^{+0.039}_{-0.067}$
NGC 1795	$0.27^{+0.14}_{-0.12}$	$18.45^{+0.14}_{-0.10}$	$1.541^{+0.383}_{-0.344}$	$0.008^{+0.001}_{-0.004}$	$0.500^{+0.029}_{-0.029}$

Note. Most likely cluster parameters listed are the maximum posterior probability, given our priors. Conservative uncertainties listed are the 16 and 84 percentiles of the PDFs (see Figures 11 and 12).

over an age range of ∼1–2.5 Gyr (the exact age limits depend on the cluster). In other words, a younger age will be derived from a stellar population with true core overshooting strength that is lower than the model (see also the bottom two panels of Figure 7). Researchers constraining core overshooting (or perhaps any stellar evolutionary parameter) should be vigilant of possible degeneracies and their implications on their results.

We combined the marginalized PDFs of core overshooting strength (by summing the log likelihoods of all six clusters), and evaluated the resulting maximum posterior probability, the 16th, and the 84th quartiles. Given the PARSEC models, we find the most likely value of core overshooting for clusters with ages ∼1.3–2.0 Gyr is $\Lambda_c = 0.500^{+0.016}_{-0.134}\, H_p$. Our results fit within the previous work of Girardi et al. (2009), but are slightly more efficient values than expected in the relationships presented by Claret & Torres (2016).

6. Conclusions

Convection is an important but uncertain aspect of stellar evolution. We show that uncertainty in the strength of core overshooting can result in ∼150 Myr uncertainty in core burning lifetimes for stars with mass ∼1–2$M_\odot$. This timescale is nearly as long as the expected SF duration invoked as an explanation of extended MSTOs in the MCs, the lifetimes of massive helium-burning stars in nearby dwarf galaxies, and the lifetimes of important, but short-lived stellar phases like the TP-AGB.

We have introduced a robust method to constrain uncertain stellar evolutionary parameters and applied the method to simultaneously fit foreground extinction, distance, age, metallicty, and the strength of core overshooting using LMC clusters with a narrow range of previously reported ages (1.30–2.04 Gyr). We report the most likely cluster parameters as well as the correlations between the parameters. We show several strong correlations, even when fixing Λ_c to the canonical PARSEC value. Metallicity appears correlated with extinction, distance, and age for each cluster. When varying Λ_c, we find a strong correlation with increasing core overshooting strength and increasing age, mirroring trends reported in the literature.

This study is a first step in systematically constraining uncertain aspects of stellar evolution using MC clusters. We expected clusters within the range of ∼1.5 Gyr MSTO would have core overshooting strength at roughly $0.4\, H_p < \Lambda_c < 0.5\, H_p$. Our findings on the most likely values were expected; however, the complex shape of the PDFs and the strength of the degeneracies between Λ_c and age were perhaps surprising. We will apply this fitting method to MC clusters at various literature-derived ages to further test whether or not core overshooting does in fact increase with increasing mass.

We will explore other means to investigate the relationship between core overshooting and age. For example, we will try to break the correlation by imposing stronger prior distributions. One way to do this would be to use Milky Way open clusters that have independently derived ages, such as from white dwarf cooling sequences or gyrochronology (e.g., Barnes 2007; Jeffery et al. 2011; Tremblay et al. 2014).

Applying more independent measurements to constrain prior distributions should also tighten the PDFs. Such measurements would be especially beneficial for metallicity, given its correlations with other cluster parameters, and the multiple-peaked marginalized PDFs (see NGC 1718 and NGC 2213 in Figure 12). For example, including spectroscopically determined metallicities of a sample of stars in the clusters would help further constrain Λ_c, or any other physical model, such as rotation. In light of the correlations found between the cluster parameters, we urge caution when using results from isochrone fitting methods that fix or adopt values before actually fitting.

P.R. thanks Charlie Conroy, Benjamin Johnson, and Phillip Cargile for many helpful discussions. This material is based upon work supported by the National Science Foundation under Award No. 1501205. Support for this work was also provided by NASA through grant number AR-13901 from the Space Telescope Science Institute. All of the data presented in this paper were obtained from the Mikulski Archive for Space Telescopes (MAST). STScI is operated by the Association of Universities for Research in Astronomy, Inc., under NASA contract NAS5-26555. Support for MAST for non-*HST* data is provided by the NASA Office of Space Science via grant NNX09AF08G and by other grants and contracts. Computations in this paper were run on the Odyssey cluster supported by the FAS Division of Science, Research Computing Group at Harvard University.

This research has made use of NASA's Astrophysics Data System, NASA/IPAC Extragalactic Database (NED), which is operated by the Jet Propulsion Laboratory, California Institute of Technology, under contract with the National Aeronautics and Space Administration, the IPython package (Pérez & Granger 2007), Astropy, a community-developed core Python package for Astronomy (Astropy Collaboration et al. 2013), TOPCAT, an interactive graphical viewer and editor for tabular data (Taylor 2005), SciPy (Jones et al. 2014), and NumPy (Van Der Walt et al. 2011).

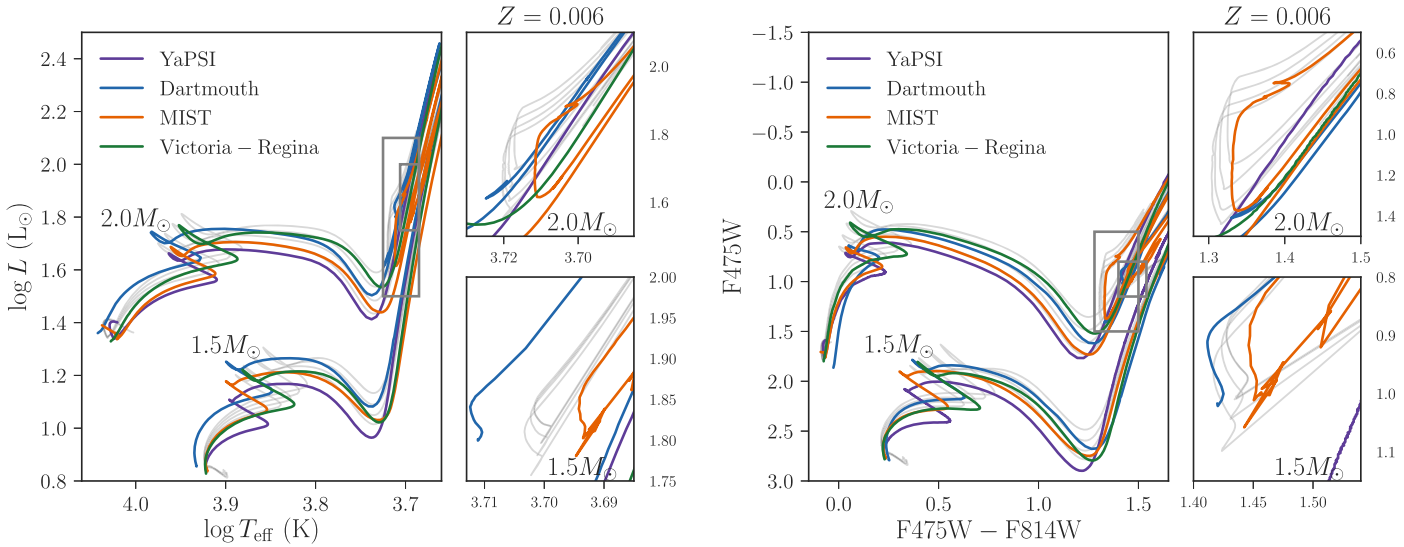

Figure 13. Left: Hertzsprung–Russell diagram (left) and CMD (right) showing model stellar evolutionary tracks at two masses from different stellar modeling groups. In gray are the PARSEC tracks from Figure 5.

Table 8
Stellar Tracks from Five Modeling Groups

Source	Z_i	Y_i	$\alpha_{\rm MLT}$	Heavy Element Mixture
PARSEC V1.2S	0.006	0.259	1.74	Grevesse & Sauval (1998), Caffau et al. (2011)
YaPSI	0.005416	0.25	1.91804	Grevesse & Sauval (1998)
Victoria-Regina	0.006	0.247	1.89	Anders & Grevesse (1989), Grevesse et al. (1990, 1991)
Dartmouth	0.006	0.254	1.938	Grevesse & Sauval (1998)
MIST	0.00582	0.2577	1.82	Asplund et al. (2009)

Note. Stellar evolution track parameters of those shown in Figure 13.

Appendix
Uncertainties across Stellar Modeling Groups

We motivated this study with the statement that stellar evolution models are fundamental to nearly all studies in astrophysics and implied the importance of a quantitative understanding of uncertainties within stellar models. However, this study begs the question of what to do with vastly different predictions *across* stellar modeling groups. Stellar models (i.e., tracks or isochrones) are seldom published with any estimates of uncertainties, leaving researchers who use the models to fend for themselves (or assume infinite precision). In one strategy, researchers have applied models from different stellar evolution groups and considered differences in predictions to be systematic uncertainties of stellar models (e.g., Dolphin 2012; Weisz et al. 2014). Until stellar evolution groups provide probabilistic tracks and isochrones to the community, this is probably the most reasonable means to interpret results from models that use different input physical assumptions.

However, from the perspective of a stellar evolutionist, differences between a stellar model from one group to another is not a source of uncertainty. In fact, the choices made in each group are very deliberate. For example, models rest on some solar calibration to scale abundances heavier than He, but differ on the source of the calibration and therefore, the initial solar metallicity. Models also differ in their treatment (i.e., applications of 1D approximations) of convection, applying different mixing length parameter values ($\alpha_{\rm MLT}$; which are also calibrated to a solar model) as well as different treatments of convective overshooting, from MLT-like (e.g., YaPSI and Dartmouth; Dotter et al. 2008; Spada et al. 2017) to a diffusion approximation (e.g., MIST, Victoria-Regina VandenBerg et al. 2006; Choi et al. 2016). Still, each of the above listed modeling groups report that the effective strength in core convective overshooting is $\Lambda_c \sim 0.4\ H_p$.

To illustrate a sample of the different predictions between stellar modeling groups, Figure 13 is based on Figure 5 but with the PARSEC core overshooting grid in gray, and Victoria-Regina,[11] YaPSI,[12] Dartmouth,[13] and MIST[14] tracks overplotted. For the CMD in the right panel, we applied the same bolometric corrections as we have for PARSEC (see Section 4.1.2 and Girardi et al. 2008) for Victoria-Regina and YaPSI who publish isochrones in *HST* filter systems, but not tracks. Some specific differences between each modeling group are listed in Table 8.

Even in this limited example, the predictions from one model to another nearly cover the entire HRD and CMD space of the PARSEC core overshooting grid (though the track with $\Lambda_c = 0.5$ is much more likely to explain the data than the other overshooting values plotted). However, the predicted CMD morphologies are different enough that they may not be degenerate, especially considering any differences in predicted

[11] http://www.cadc-ccda.hia-iha.nrc-cnrc.gc.ca/community/VictoriaReginaModels/
[12] http://vo.aip.de/yapsi/description_2016.html
[13] http://stellar.dartmouth.edu/%7Emodels/fehp00afep0.html
[14] http://waps.cfa.harvard.edu/MIST/model_grids.html

lifetimes (not shown) between modeling groups. With high signal-to-noise observations, a large number of stars, and filters chosen to maximize the separation of CMD features, one could distinguish between the different predicted CMD morphologies from each modeling group.

The differences due to the careful decisions and their implementations between one stellar modeling group and another are model predictions that can and should be systematically tested against observations. The statistical (Bayesian) treatment we have presented is applicable for exactly this purpose because it is agnostic of the stellar model and uncertain parameters. With a uniform binning scheme, only one further step would be necessary to compare one model to another, which is to calculate the model evidence.

References

Anders, E., & Grevesse, N. 1989, GeoCoA, 53, 197
Arnett, W. D., Meakin, C., Viallet, M., et al. 2015, ApJ, 809, 30
Asplund, M., Grevesse, N., Sauval, A. J., & Scott, P. 2009, ARA&A, 47, 481
Astropy Collaboration, Robitaille, T. P., Tollerud, E. J., et al. 2013, A&A, 558, A33
Barmina, R., Girardi, L., & Chiosi, C. 2002, A&A, 385, 847
Barnes, S. A. 2007, ApJ, 669, 1167
Bastian, N., Niederhofer, F., Kozhurina-Platais, V., et al. 2016, MNRAS, 460, L20
Basu, S., Chaplin, W. J., Elsworth, Y., New, R., & Serenelli, A. M. 2009, ApJ, 699, 1403
Baumgardt, H., Parmentier, G., Anders, P., & Grebel, E. K. 2013, MNRAS, 430, 676
Bertelli, G., Girardi, L., Marigo, P., & Nasi, E. 2008, A&A, 484, 815
Bertelli, G., Nasi, E., Girardi, L., et al. 2003, AJ, 125, 770
Bica, E., Bonatto, C., Dutra, C. M., & Santos, J. F. C. 2008, MNRAS, 389, 678
Böhm-Vitense, E. 1958, ZAp, 46, 108
Bressan, A., Fagotto, F., Bertelli, G., & Chiosi, C. 1993, A&AS, 100, 647
Bressan, A., Marigo, P., Girardi, L., et al. 2012, MNRAS, 427, 127
Bressan, A., Marigo, P., Girardi, L., Nanni, A., & Rubele, S. 2013, in European Physical Journal Web of Conf. 43, Aging Low Mass Stars: From Red Giants to White Dwarfs, ed. J. Montalbán, A. Noels, & V. Van Grootel (Trieste: EDP), 3001
Bressan, A. G., Chiosi, C., & Bertelli, G. 1981, A&A, 102, 25
Brocato, E., Castellani, V., Di Carlo, E., Raimondo, G., & Walker, A. R. 2003, AJ, 125, 3111
Cabrera-Cano, J., & Alfaro, E. J. 1990, A&A, 235, 94
Caffau, E., Ludwig, H.-G., Steffen, M., Freytag, B., & Bonifacio, P. 2011, SoPh, 268, 255
Castelli, F., & Kurucz, R. L. 2004, arXiv:astro-ph/0405087
Chabrier, G. 2003, PASP, 115, 763
Chen, Y., Girardi, L., Bressan, A., et al. 2014, MNRAS, 444, 2525
Choi, J., Dotter, A., Conroy, C., et al. 2016, ApJ, 823, 102
Claret, A., & Torres, G. 2016, A&A, 592, A15
Correnti, M., Goudfrooij, P., Kalirai, J. S., et al. 2014, ApJ, 793, 121
Dalcanton, J. J., Williams, B. F., Lang, D., et al. 2012, ApJS, 200, 18
Dalcanton, J. J., Williams, B. F., Seth, A. C., et al. 2009, ApJS, 183, 67
de Grijs, R., Wicker, J. E., & Bono, G. 2014, AJ, 147, 122
Deheuvels, S., Michel, E., Goupil, M. J., et al. 2010, A&A, 514, A31
Demarque, P., Sarajedini, A., & Guo, X.-J. 1994, ApJ, 426, 165
Demarque, P., Woo, J.-H., Kim, Y.-C., & Yi, S. K. 2004, ApJS, 155, 667
Dolphin, A. E. 2000, PASP, 112, 1383
Dolphin, A. E. 2002, MNRAS, 332, 91
Dolphin, A. E. 2012, ApJ, 751, 60
Dolphin, A. E. 2016, ApJ, 825, 153
Dotter, A., Chaboyer, B., Jevremović, D., et al. 2008, ApJS, 178, 89
Gallart, C., Zoccali, M., & Aparicio, A. 2005, ARA&A, 43, 387
Girardi, L., Bertelli, G., Bressan, A., et al. 2002, A&A, 391, 195
Girardi, L., Bressan, A., Bertelli, G., & Chiosi, C. 2000, A&AS, 141, 371
Girardi, L., Dalcanton, J., Williams, B., et al. 2008, PASP, 120, 583
Girardi, L., Rubele, S., & Kerber, L. 2009, MNRAS, 394, L74
Glatt, K., Grebel, E. K., & Koch, A. 2010, A&A, 517, A50
Gonzaga, S., Hack, W., Fruchter, A., & Mack, J. 2012, The DrizzlePac Handbook (Baltimore: STScI)
Goodwin, S. P., & Kroupa, P. 2005, A&A, 439, 565
Goudfrooij, P., Girardi, L., Kozhurina-Platais, V., et al. 2014, ApJ, 797, 35
Goudfrooij, P., Puzia, T. H., Kozhurina-Platais, V., & Chandar, R. 2011, ApJ, 737, 3
Grevesse, N., Lambert, D. L., Sauval, A. J., et al. 1990, A&A, 232, 225
Grevesse, N., Lambert, D. L., Sauval, A. J., et al. 1991, A&A, 242, 488
Grevesse, N., & Sauval, A. J. 1998, SSRv, 85, 161
Guenther, D. B., Demarque, P., & Gruberbauer, M. 2014, ApJ, 787, 164
Jeffery, E. J., von Hippel, T., DeGennaro, S., et al. 2011, ApJ, 730, 35
Jones, E., Oliphant, T., & Peterson, P. 2014, SciPy, http://www.scipy.org
Kalirai, J. S., Richer, H. B., Anderson, J., et al. 2012, AJ, 143, 11
Kerber, L. O., Santiago, B. X., & Brocato, E. 2007, A&A, 462, 139
Komatsu, E., Smith, K. M., Dunkley, J., et al. 2011, ApJS, 192, 18
Kozhurina-Platais, V., Demarque, P., Platais, I., Orosz, J. A., & Barnes, S. 1997, AJ, 113, 1045
Kroupa, P., & Petr-Gotzens, M. G. 2011, A&A, 529, A92
Madau, P., & Dickinson, M. 2014, ARA&A, 52, 415
Marigo, P., Girardi, L., Bressan, A., et al. 2008, A&A, 482, 883
Marks, M., & Kroupa, P. 2011, MNRAS, 417, 1702
Marks, M., Kroupa, P., & Oh, S. 2011, MNRAS, 417, 1684
McQuinn, K. B. W., Skillman, E. D., Cannon, J. M., et al. 2010, ApJ, 724, 49
Melbourne, J., Williams, B. F., Dalcanton, J. J., et al. 2012, ApJ, 748, 47
Milone, A. P., Bedin, L. R., Piotto, G., & Anderson, J. 2009, A&A, 497 755
Milone, A. P., Marino, A. F., Bedin, L. R., et al. 2016, MNRAS, 455, 3009
Mucciarelli, A., Origlia, L., & Ferraro, F. R. 2007, AJ, 134, 1813
Niederhofer, F., Bastian, N., Kozhurina-Platais, V., et al. 2016, A&A, 586, A148
Overbeek, J. C., Friel, E. D., Donati, P., et al. 2017, A&A, 598, A68
Pérez, F., & Granger, B. E. 2007, CSE, 9, 21
Perren, G. I., Vázquez, R. A., & Piatti, A. E. 2015, A&A, 576, A6
Piatti, A. E., Keller, S. C., Mackey, A. D., & Da Costa, G. S. 2014, MNRAS, 444, 1425
Pietrinferni, A., Cassisi, S., Salaris, M., & Castelli, F. 2004, ApJ, 612, 168
Ribas, I., Jordi, C., & Giménez, Á 2000, MNRAS, 318, L55
Rosenfield, P., Marigo, P., Girardi, L., et al. 2016, ApJ, 822, 73
Salaris, M., & Cassisi, S. 1997, MNRAS, 289, 406
Salpeter, E. E. 1955, ApJ, 121, 161
Sarajedini, A., von Hippel, T., Kozhurina-Platais, V., & Demarque, P. 1999, AJ, 118, 2894
Schlafly, E. F., & Finkbeiner, D. P. 2011, ApJ, 737, 103
Schroder, K.-P., Pols, O. R., & Eggleton, P. P. 1997, MNRAS, 285, 696
Smartt, S. J. 2015, PASA, 32, e016
Sollima, A., Beccari, G., Ferraro, F. R., Fusi Pecci, F., & Sarajedini, A. 2007, MNRAS, 380, 781
Spada, F., Demarque, P., Kim, Y.-C., Boyajian, T. S., & Brewer, J. M. 2017, ApJ, 838, 161
Tang, J., Bressan, A., Rosenfield, P., et al. 2014, MNRAS, 445, 4287
Taylor, M. B. 2005, in ASP Conf. Ser. 347, Astronomical Data Analysis Software and Systems XIV, ed. P. Shopbell, M. Britton, & R. Ebert (San Francisco, CA: ASP), 29
Torres, G., Andersen, J., & Giménez, A. 2010, A&ARv, 18, 67
Tremblay, P.-E., Kalirai, J. S., Soderblom, D. R., Cignoni, M., & Cummings, J. 2014, ApJ, 791, 92
Van Der Walt, S., Colbert, S. C., & Varoquaux, G. 2011, CSE, 13, 22
VandenBerg, D. A., Bergbusch, P. A., & Dowler, P. D. 2006, ApJS, 162, 375
von Hippel, T., Jefferys, W. H., Scott, J., et al. 2006, ApJ, 645, 1436
Weisz, D. R., Dolphin, A. E., Skillman, E. D., et al. 2014, ApJ, 789, 147
Williams, B. F., Lang, D., Dalcanton, J. J., et al. 2014, ApJS, 215, 9
Woo, J.-H., & Demarque, P. 2001, AJ, 122, 1602
Woo, J.-H., Gallart, C., Demarque, P., Yi, S., & Zoccali, M. 2003, AJ, 125, 754
Yi, S., Demarque, P., Kim, Y.-C., et al. 2001, ApJS, 136, 417